# A COMBINATION OF COMPUTER VISION AND OBJECT BASED IMAGE SEGMENTATION TO MODEL FOREST BIOMASS AND CARBON STOCK IN TROPICAL RAIN FOREST OF KELAY, INDONESIA

APRI DWI SUMARAH
February, 2014

SUPERVISORS:
Dr. Y. A. Hussin
Dr. M.J.C. Weir

# A COMBINATION OF COMPUTER VISION AND OBJECT BASED IMAGE SEGMENTATION TO MODEL FOREST BIOMASS AND CARBON STOCK IN TROPICAL RAIN FOREST OF KELAY, INDONESIA

APRI DWI SUMARAH
Enschede, The Netherlands, February, 2014

Thesis submitted to the Faculty of Geo-Information Science and Earth Observation of the University of Twente in partial fulfilment of the requirements for the degree of Master of Science in Geo-information Science and Earth Observation.
Specialization: Natural Resources Management

SUPERVISORS:
Dr. Y. A. Hussin
Dr. M.J.C. Weir

THESIS ASSESSMENT BOARD:
Dr. Ir. C. A. J. M. de Bie (Chair)
Dr. M. Gerke (External Examiner, University of Twente – ITC)

# ABSTRACT

Forests play an important role in climate change issue by their ability to sequester and store carbon in the living biomass of forest trees. Thus, accurate above ground biomass estimation is essential element for measuring and monitoring carbon stock under the REDD+ mechanism. High spatial resolution three dimensional (3D) aerial photographs offers a new prospective for above ground biomass estimation which is low cost. This study aims to investigate a potential approach for modelling of above ground biomass and carbon stock in tropical rain forest using the combination of computer vision technologies and object based image segmentation on airborne images.

The Structure from Motion (SfM) of computer vision techniques was applied to define the 3D location of point clouds of each object in a scene from a sequence of airborne images that are overlapping. 3D point clouds were processed to generate the canopy height model (CHM) using subtraction of digital terrain model and digital surface model. A multi-resolution algorithm approach was used for automated object based image segmentation to derive crown projection area. The estimation of field above ground biomass (AGB) was calculated employing field measured diameter at breast height (DBH), height and wood specific gravity using generic allometric equation and then the AGB was converted into carbon stock.

The CHM derived from 3D point clouds was able to explain around 77.39% of the field measured height variability. The segmentation of individual tree crown that employed multi-resolution method resulted 64% of accuracy based on the goodness measure approach (D). The log transformed regression between CHM, CPA and AGB was established with $R^2$ about 56.66%. Using this model, the amount of AGB was around 190.51 $MgHa^{-1}$ or converted into carbon stock was about 89.54 $MgCHa^{-1}$. The alternative model between log transformed DBH, CHM and AGB was also assessed with $R^2$ 97.45%.

Generally, despite the difficulty to extract individual crown canopy, this study demonstrated the new approach of remote sensing using high resolution 3D photographs to derive canopy height model with properties comparable to LiDAR. Further research is recommended to improve the accuracy of CHM by combining aerial point clouds with LiDAR data and explore other approaches for image segmentation.



**Keywords:** Above ground biomass, Airborne image, Structure from Motion, Multi-resolution, Canopy height model, Crown projection area

# ACKNOWLEDGEMENTS

I am sincerely grateful to the Netherlands Government and the Netherlands organisation for international cooperation in higher education (NUFFIC) for granting me a scholarship to study in the Netherlands. I would like to acknowledge my institution in Indonesia, Ministry of Forestry for providing any supports during my scholarship and M.Sc. enrollment application process.

I am grateful to ITC, University of Twente for facilitating my study and research. And special thanks go to all NRM staff who gave me a good academic process to learn new skills and techniques of GIS and Remote Sensing.

My greatest gratitude and appreciation goes to my first supervisor Dr. Yousif Hussin for his valuable guidance, constructive feedback and comment from the very beginning till the completion of this study. I would like to thank my second supervisor Dr. Michael Weir and also as NRM course director, thank you for your valuable advice, feedback and continuous support during my study. I would like to thank Dr. Kees de Bie for his comment and suggestion during my proposal defense and mid-term which help to improve my research.

I would like to acknowledge to The Nature Conservancy Indonesia for providing digital airborne data and other necessary data and the arrangement of the field work. I am thankful to PT. Karya Lestari for providing technical support during the fieldwork. I would like to thanks to my fieldwork mate Jarot Pandu Panji Asmoro who shared together the hardship times and cheerful during field work.

To my NRM and GEM students batch 2012 – 2014, thank you a lot for being a part of you guys. Many thanks for the memorable time we were together, especially for our "pie day". To my Indonesian fellow thanks for your all the supports during this whole time and for making me feel at home.

My deepest gratitude goes to my family, especially my parents, my wife and my daughter for their prayers and moral supports during this whole time. You have always special place in my heart

# TABLE OF CONTENTS

# LIST OF FIGURES

# LIST OF TABLES

# LIST OF APPENDICES

# 1. INTRODUCTION

## 1.1. Background

Forest as a renewable natural resource is one of the potential sources of wealth that provides various economic, social and environmental benefits. This is especially the case in the tropical forest, which covers around 44% of global forest area (FAO, 2010). Tropical forests play an important role in regulating global weather (Butler, 2012) and generate a substantial number of goods and services benefit to humankind (Pearce, 2001). Nevertheless, the area of tropical forest area is declining because of various problems.

Forest degradation and deforestation have emerged as important issues in the forestry sector. Many efforts have been made to combat tropical rain forest degradation and deforestation. Meanwhile, there are many indicators that the reduction and degradation of tropical rain forest is still continuing. According to World Bank, in Indonesia within 20 years (1990 – 2010) the depleted forest area is around 24,113,000 ha (World Bank, 2013).Logging is one factor that contributes for forest degradation. Over the last ten years, in Indonesia, the area of primary forest decreased by about 0.4 percent per year as a result of selective logging and other human interventions (FAO, 2010). Moreover, Indonesia is a country with the annual largest net loss of forest area (FAO, 2010).

Forests play an important role in climate change adaptation and mitigation. In an attempt to preserve forest's carbon, the UNFCCC launched Reducing Emission from Deforestation and Forest Degradation (REDD), is a mechanism that is directly linked to financial incentives for conservation of carbon stored in forests (CIFOR, 2009). REDD aims to slow down the rate of deforestation and forest degradation of tropical forest in developing countries (Bársony et al., 2011). The forest management can be stimulated through the REDD scheme. REDD generates carbon credit mechanism based on the performance of new approaches to forest and forest management for reducing carbon loss compare to a defined baseline (MoF, 2008). Thus, REDD can enable the increase of carbon stock in forests and contribute to assist in global climate change mitigation. Since, deforestation and forest degradation release carbon, Indonesia has a significant incentive to take part in the REDD scheme through retaining the country's forests to obtain financial benefits.

Financial incentives for applying REDD mechanism may provide motivation for implementing sustainable forest management (SFM) (Braatz, 2008). Sustainable forest management is an indispensable concept that attempts to strike a balance between environment, social and economic components. The International Tropical Timber Organization (ITTO) defines SFM as "a process of managing forests to achieve one or more clearly specified objectives of management with regard to the production of a continuous flow of desired forest products and services, without undue reduction of its inherent values and future productivity and without undue undesirable effects on the physical and social environment" (ITTO, 2000).

Indonesia, with 51.7% of the total land is covered by forest (World Bank, 2013), also implements SFM to maintain the sustainability of its forest. This indicates that Indonesia has potential carbon stock as the natural resource to support economic development. Therefore, Indonesia has an opportunity to contribute to reducing emission under REDD scheme. In addition, forestry sector is an important resource and also contributes to the national income since the commercial logging was allowed by Indonesian Basic Forestry Law in 1967 (Barr et al., 2006).

Selective logging is a commonly employed method of commercial timber production. In Indonesia, the concession holders commonly apply the Indonesian selective logging (TPTI[1]) as the silviculture system. TPTI (as abbreviated in Indonesian Language) stipulates that all timber trees (except protected trees) with a diameter greater than 50 cm DBH (diameter at breast height) can be harvested with a polycyclic felling rotation of 35 years (Priyadi, 2007). The timber harvesting regulation of TPTI is not allowed to exceed the natural growth of trees. TPTI aims to regulate and increase the forest production - both quality and quantity - on the logged over area for the next harvesting cycle, thus the mixed forest could be managed to produce a sustainable timber production (Muhdi, 2005).

As a consequent of timber harvesting is releasing the carbon stored in the aboveground living biomass of trees. Then, the challenge for Indonesia is to have the ability to quantify the emission from timber harvesting activities (MoF, 2008). In term of carbon stock monitoring and verification under REDD mechanism in the forest, many methods have been implemented. In order to have appropriate carbon monitoring, the combination of field measurement and remote sensing techniques are essential for calibrating and validating spatial estimates of aboveground biomass / carbon stock (Goetz & Dubayah, 2011).

High spatial airborne optical images of vegetation in 3D has become a new opportunity for carbon measurement (Goetz & Dubayah, 2011). The characteristics of tree are essential for carbon measurement and these can be derived from airborne images. The tree height as a critical factor for above ground biomass and carbon stock estimation can be produced through stereo pair and multiple stereo pair of digital imagery captured from aircraft (Brown et al., 2005; Korpela, 2004; Tao et al., 2011). The individual tree crown is also very important for biomass which could be derived by object based image classification from aerial images. Hence, knowing the potential of the combination of computer vision techniques and object based segmentation offers an alternative for biomass estimation in the tropical rain forest.

### 1.2. Overview of techniques

There are several approaches to measure biomass, which are based on Physiological Process, Remote Sensing and Geographic Information System, Carbon Flux measurements, Forest Yield and Forest Inventory. These methods were reviewed and summarized by Qureshi et al. (2012). Among those approaches, the forest yield method is most accurate and effective, but it is time inefficient. The destructive method namely the harvesting and weighing of trees is the only direct and accurate way to measure aboveground biomass; however, this method is generally impractical to be applied. The use of allometric equation as non-destructive method establishes the relationship between diameter breast high (DBH) and tree height and can be used to quantify forest carbon stock based on field measurements (Gibbs et al., 2007).

The Remote Sensing based approach provides an alternative to traditional field-based methods and gives a cost effective and faster method than the obsolete way with an acceptable degree of accuracy in the estimation of biomass (Gibbs et al., 2007). None of remote sensing instruments are directly able to estimate forest biomass. Therefore, an adequate number of field measurements are needed in order to develop and evaluate the forest biomass modelling. Thus, a combination of remote sensing methods and field measurements should preferably be used for accurate biomass assessment (Drake et al., 2003).

[1] TPTI stand for *Tebang Pilih Tanam Indonesia* or Indonesian Selective logging (Act No. P.9/VI-BPHA/2009).

Several researches have been conducted to estimate forest above ground biomass/carbon using various types of digital remote sensing imagery, such as NOAA-AVHRR and MODIS for coarse optical spatial resolution, Landsat and ASTER for moderate spatial resolution and IKONOS, Quickbird, Geoeye and Worldview for very high spatial resolution studies. The physical dimensions of trees can be sensed accurately using very high resolution satellite (VHRS) images. Because the aboveground biomass directly correlates to the physical tree dimensions, this approach results in highly accurate estimates of biomass and carbon sequestration estimations (Gonzalez et al., 2010). Nevertheless, the effect of shadow, sun elevation angle and off-nadir viewing angle cannot be tackled by the high resolution satellite images.

LiDAR (Light Detection And Ranging) remote sensing sensor is promising technique for the estimation of above ground biomass in a variety of forest types (temperate and tropical) (Drake et al., 2003). Airborne LiDAR estimates forest carbon with lower uncertainty and higher accuracy than VHRS data (Gonzalez et al., 2010). However, the application of airborne LiDAR sensor is costly, especially if required a high spatial resolution and the points cloud density of LiDAR data is low (Tao et al., 2011). Furthermore, it needs a specialized technical expertise to process and analyse the data (Gonzalez et al., 2010).

Airborne images combine with Structure from Motion (SfM) of computer vision offers a new perspective in photogrammetry and offers an alternative with a unique ability to measure the structure of forest vegetation either in 2D or 3D. The SfM as a state-of-the-art computer vision technique has initiated the comeback of photogrammetry (Lisein et al., 2013). Moreover, the SfM has an advantage that can produce higher point cloud over LiDAR data with cost effective method of estimation (Dandois & Ellis, 2013; Järnstedt et al., 2012; Leberl et al., 2010). Thus, the availability of digital airborne images has opened the possibility to assess the characteristic of forest, since the costs of acquiring and analyzing of high-accuracy digital images can be reduced (Korpela, 2004).

### 1.2.1. Aerial photograph and how it works

Airborne imagery is the one economical method of remote sensing for taking picture of earth surface from the air using flying platforms. Historically it was the first of remote sensing method, and this method is still used widely with a significant improvement on its technology (platforms and camera).

Generally, there are two types of aerial photography: vertical and oblique (Wolf & Dewitt, 2000). Vertical images are taken with the optical axis of the camera is perpendicular to the ground. Oblique aerial photography is captured with camera axis intentionally tilted away from vertical. Vertical imagery is usually used for mapping purpose, because of its map-like characteristics.

Mostly, the vertical aerial images are captured along a series flight line of the aircraft. The images are normally recorded along the flight line so that each successive photograph will duplicate or overlap part of previous image. The overlapping along the flight line is called forward overlap and common area of a pair image in a flight line is called stereoscopic overlap. This pair is called a stereo pair, which is normally the amount of overlapping between 55%-60% (Wolf & Dewitt, 2000). There is also a lateral overlapping between flight lines which normally are around 30% (Figure 1).

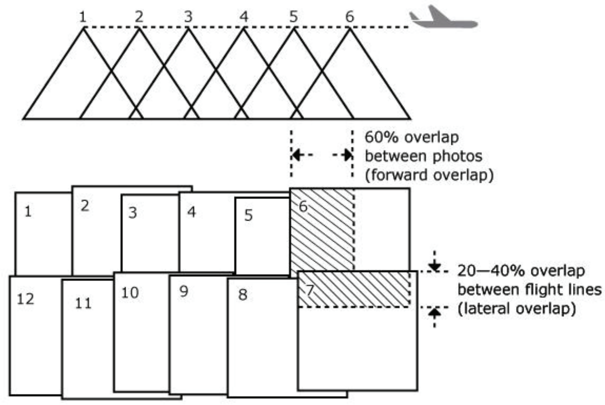


Figure 1: Illustration of flight line and image overlapping
*Source: Natural Resources Canada (www.nrcan.gc.ca)*

When the overlapping pairs of image are taken, the aerial photograph can provide a 3D terrain model (Figure 2). This 3D view is possible generated by the effect of parallax, thus it provides opportunity to analyze the characteristic of objects horizontally (2D) and vertically (3D). Parallax is the apparent change in relative positions of objects caused by a change in capturing position (Wolf & Dewitt, 2000) (Figure 3).

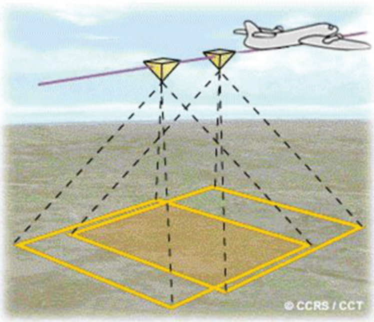


Figure 3: Illustration of stereo pair image.
*Source: Natural Resources Canada*

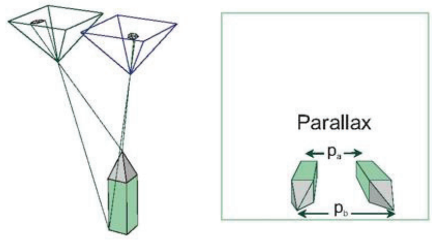


Figure 2: Illustration of Parallax
*Source: ITC*

The measurement of the difference in position (displacement) is basic input for elevation calculation. In this way the X,Y,Z coordinates of many points can be measured. In this way a Digital Surface Model (DSM) can be obtained through digital photogrammetry (Fabris & Pesci, 2005; Pulighe & Fava, 2013).

Compared to analogue photogrammetric technique, the SfM approach based on computer vision techniques are able automatically to determine scene geometry, camera calibration, position and orientation from overlapping images even from un-ordered collection of images (Snavely et al., 2007). As a result the 3D point clouds and camera orientations are further used for multi-view dense image matching (Lisein et al., 2013). A modern digital photogrammetry algorithm is based on four innovations, these are i) cost-free increasing in image overlap, ii) improving radiometry, iii) multi-view image matching, iv) making complex algorithm using the Graphic Processing Unit (Leberl et al., 2010).This approach has been estimated can produce more detailed data with geometric accuracy comparable to LiDAR data (Lisein et al., 2013).

### 1.3. Application of aerial photography to acquire data for forest biophysical characteristics estimation

Airborne imagery has a clear potential to enable the estimation of forest biomass and timber volume modelling. Airborne imagery is an essential remote sensing data source which could produce base maps to perform environmental analysis with high spatial and temporal resolution (Lillesand et. al., 2008). This remote sensing method has widely been applied for biomass mapping for many years (Chen et al., 2012; Tiwari & Singh, 1984). In contrast to optical remote sensing data and LiDAR data, aerial photography has particular characteristics, such as high point cloud and high geo-location accuracy, to assess vegetation characteristic and derive forest biomass at multiple scales, from individual trees to regional area (Korpela, 2004). Gibbs et al. (2007) and Leberl et al. (2010) have compared the airborne optical imagery and other remote sensing instrument to estimate forest biomass that the use of this method can minimize time and cost for forest inventory data collection. The aerial photographs were used to estimate aboveground biomass in temperate forest (Tiwari & Singh, 1984; Dandois & Ellis, 2010), estimate aboveground biomass in tropical forest (Okuda et al., 2004), identify tropical forest tree species (Valérie & Marie-Pierre, 2006), classify the species of the Australian forest (Lucas et al., 2008), measure the individual tree characteristics such as height and crown width (Järnstedt et al., 2012; Korpela, 2004).

Information on canopy height is essential for biomass assessment. It is possible to extract a canopy surface of forest from digital aerial photograph. This requires stereoscopic coverage of very high resolution imagery (Järnstedt et al., 2012). Previous research has proved that the canopy surface modelling using digital aerial photogrammetry has similar quality compare to that which is obtained by LiDAR data (e. g. Bohlin et al., 2012; Järnstedt et al., 2012; St-Onge et al., 2008).

The structure from motion (SfM) algorithm methods can be used in order to derive the heights of tree, and in this way, 3D visualization of forest structure can be generated from overlapping aerial images (Dandois & Ellis, 2010; Tao et al., 2011; Geert Verhoeven, 2011). SfM extracts key points from each image, identifies the overlapping feature among images and derives the 3D location of matching features.

Computer vision methods of SfM have been successfully applied by several researches for digital surface models (DSM), digital terrain models (DTM) and orthophoto (Baillard, 2003; Lucieer et al., 2014; Niethammer et al., 2012). 3D point clouds of wide range object or based on many sets of overlapping images can be obtained by SfM technique, which this procedure was performed by Snavely et al. (2007).

Another tree characteristic that can be extracted from airborne images is crown projection area (CPA). Object based image segmentation (OBIA) is now commonly used to derive the crown projection area of forest trees from very high resolution image (Shiba & Itaya, 2005; Walker & Briggs, 2005). The image object or the segments are the basic unit of object based image classification rather than the traditional pixel-based classification (Blaschke, 2010). OBIA classify an image based on reflectance value (color), shape, texture, size and context.

## 1.4. Problem statement and justification

The main goal of the REDD+ program to reduce carbon emission from degradation and deforestation through a good practice of sustainable forest management (UN-REDD, 2013). Thus a transparent, coherent and complete system of measurement, reporting and verification (MRV) is required to monitor carbon emission from each country. The combination of remote sensing and ground based data is considered to be essential for MRV (UNFCC, 2009). Otherwise, if remote sensing data are absent, the MRV process would be time consuming, costly and involve a lot of human effort.

A number of remote sensing based methods have been developed for forest biomass mapping. Over the last decade these methods have focused on the use of LiDAR data, polarimetric synthetic radar interferometry and hyper-spectral data (Koch, 2010). Nevertheless, most of the existing methods have high level of uncertainty, and thus accurate methods are required (Köhl et al., 2009). The very high resolution of digital imagery and 3D digital photogrammetry can provide more accurate estimation of forest biomass / carbon stock and mapping them.

Diameter breast height (DBH) and height of tree is a fundamental element for forest inventory. DBH cannot be derived automatically from airborne optical imagery. Thus, a regression relationship between DBH, crown projection area (CPA) is needed to estimate forest biomass from remote sensing approach. Crown width of tree can be derived from object-based segmentation while height can be obtained by structure from motion method using aerial photography. Thus, the individual tree information can be extracted to estimate tree biomass.

In order to estimate biomass of forest, the individual tree traits such as tree height and canopy closure can be generated from digital airborne optical image with good results. There have been previous researches examined the possibility of aerial photogrammetry combined with computer vision techniques to estimate forest and vegetation structure (Dandois & Ellis, 2013; Pouliot et al., 2002). Some previous studies also have been conducted for individual tree crown segmentation (Jing et al., 2012; Meia & Durrieub, 2004; Tsendbazar, 2011). However, those studies have not been done in the tropical rain forest.

The research described in this thesis aims to explore the possibility of accurate biomass estimation of forest from the combination between computer vision techniques and object-based image analysis using airborne optical images in a tropical environment. In addition, the complexity of tropical rain forest characteristic is very challenging to do this research. Therefore, it is anticipated that this research can contribute to provide an alternative approach of remote sensed based for biomass / carbon stock estimation in tropical forest.

## 1.5. Research objectives

The overall objective of this research is to investigate a potential approach for modelling of carbon stock in tropical rain forest using the combination of computer vision technologies and object based image segmentation based on point cloud derived from airborne optical 3D images.

### 1.5.1. Specific research objectives

1. To estimate the canopy height model and canopy crown area derived from point cloud of 3D airborne optical images and assess the accuracy of these estimations.
2. To determine the relationship among CPA, DBH, height derived from 3D airborne optical images and biomass of trees in tropical rain forest.
3. To develop a model of aboveground biomass and carbon stock estimation using high resolution of 3D airborne optical images. .
4. To estimate and map aboveground biomass and carbon stock from point clouds of 3D airborne optical images.

## 1.6. Research question

1. How accurately can height and CPA of individual tree of tropical rain forest be estimated from the point clouds extracted from 3D airborne images?
2. What is the relationship among diameter, CPA, height derived from 3D point clouds of optical 3D airborne images and aboveground biomass in the study area?
3. How can point clouds extracted from 3D optical airborne images be used to improve the estimation of above ground biomass / carbon stock of tropical rain forest?
4. How well do model developed by a point cloud extracted from 3D optical airborne images to estimate above ground biomass / carbon stock of the study area?
5. How much above ground biomass / carbon stock are stored in the tropical rain forest of study area?

## 1.7. Research Hypotheses

1. Ho: Accuracy of height and CPA of individual tree estimated from point cloud of 3D optical airborne images are more than 80%.

   Ha: The above accuracy is less than 80%.
2. Ho: There is no significant difference between the height of tree measured from field and from point cloud of 3D airborne images.

   Ha: There is a significant difference between the height of tree measured from field and from point cloud of 3D airborne images.
3. Ho: There is a significant relationship between CPA, height estimated from point cloud of 3D optical airborne images and biomass of tropical rain forest trees in the study area.

   Ha: There is no significant relationship between CPA, height estimated from point cloud of 3D optical airborne images and biomass of tropical rain forest trees in the study area.

# 2. STUDY AREA

## 2.1. Criteria for study area selection

The study area was in Kelay concession that is the one of the Berau Forest Carbon Program (BFCP). The BFCP was selected by Ministry of Forestry of Republic of Indonesia as the one of national REDD demonstration program. The BFCP project is supported by The Nature Conservancy Indonesia (TNC) through program design and development including providing data for working group. Thus, the data availability was also considered as the study area selection.

## 2.2. Overview of Kelay Unit Concession

Kelay Forest Management Unit is a part of a private owned forest concession company named PT. Karya Lestari that covers about 49,123 ha of production forest. Since 1999, Kelay concession has been managed by PT. Karya Lestari and allowed to continue their forest management activities in Kelay concession until the end of 2054. In order to improve sustainable forest management for this FMU to become more effective, Kelay FMU is divided into several management units or logging blocks.

According to the Government of Indonesia, there are two classes of forest based its function in Kelay unit. Those classes are limited forest production and forest production area. The limited forest production is the forest class in which it is not allowed to harvest the trees with DBH less than 50 cm, while in the forest production class should not cut the trees under 40 cm of DBH.

## 2.3. Geographic location and climate condition

Geographically, Kelay concession area is located in Berau regency, which is one of four regencies in East Kalimantan province, Indonesia. It is situated between $01^0$ 35' 15.6" N and $01^0$ 48' 4.4" N longitude and $116^0$ 40' 12.2" E and $116^0$ 59' 46.7" E (Figure 4).

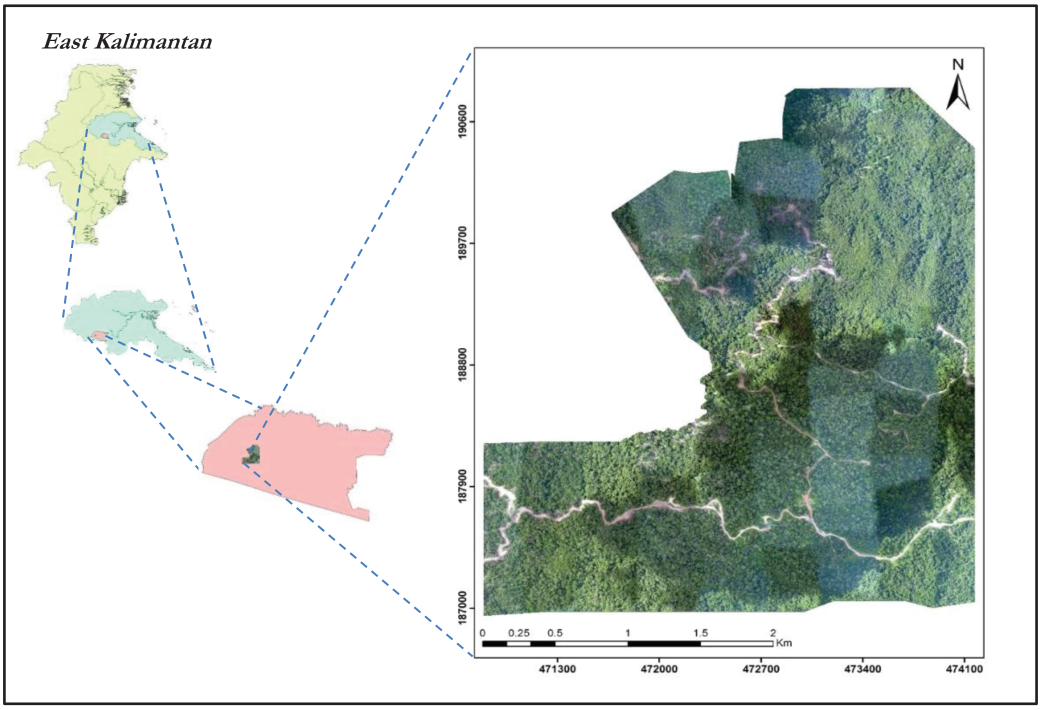


Figure 4: Location of the study area, Kelay, Berau, East Kalimantan, Indonesia

The average annual rainfall rate in Kelay is around 2179 mm or monthly rain fall rate around 181,6 mm. Based on its monthly rainfall rate (that is higher than 100 mm), Kelay is classified as type A that is a tropical rain forest where the percentage of ratio between dry and wet months is less than 14.3% (Schmidt & Ferguson, 1951). The average temperature in Kelay concession is around $26^0 – 27^0$ C with 85% air humidity.

## 2.4. Topography

The elevation in Kelay concession area is ranging between the 100 meter and 400 meter of above mean sea level. About 22% of the area is relatively flat area with slope around 0 – 8%, 10% of the area has moderate slope around 8 – 15%, then a light steep slope in 27% of area and the rest of the terrain has steep slopes exceeding 25%.

## 2.5. Land cover and vegetation

The land cover in Kelay concession consists of primary forest (15,533 ha), logged over area (32,731 ha), non-forest area (390 ha) and covered by cloud (469 ha) [2]. The logged over area is more dominant because there has been timber extraction since two decades ago (Kelay area was managed by PT. Alas Helau since 1980's). In addition, the study area is 1,185.5 ha and divided into 11 harvesting compartments or logging blocks.

The vegetation types in Kelay area is dominated by tropical rain forest trees species: *Shorea sp, Dipterocarpus sp, Quercus spp, Dryobalanops sp, Palaquium sp* and *Koompassia sp*.

[2] Based on Landsat image interpretation and analysis on 2013 (decree No.S.32/IPSDH-2/2013) by Ministry of Forestry Republic of Indonesia.

# 3. MATERIALS AND METHODS

## 3.1. Dataset and Materials

Dataset and materials were used for the study are described in the following sub-chapters

### 3.1.1. Dataset:

Airborne images were collected by Credent technology[3] simultaneously with LiDAR airborne data collection on April 2013 that were used for forest biomass estimation. The image consists of three visible bands (red, green and blue) with 10.5 cm of spatial resolution (Table 1). During the data collection process the topographic map and other thematic maps were also used in the field. The aerial image was also utilised during the field work to recognise the trees on the sample plots.

Table 1. Aerial image characteristic

| Features | Descriptions |
|---|---|
| Acquisition | 06 April 2013 |
| Flying altitude | 887.833 m |
| Image Resolution | 10.5 cm |
| Camera Name | HasselbladH4D-50_50 |
| Camera Resolution | 6132x8176 |
| Focal Length | 50 mm |
| Image coordinate | WGS 84 / UTM zone 50N |

### 3.1.2. Field instruments:

The instruments that were used to enhance the data collection and fieldwork process are shown in Table 2.

Table 2. Field Instruments used for research

| No | Instruments | Purpose |
|---|---|---|
| 1 | iPAQ and GPS | Navigation and plot identification |
| 2 | Spherical densiometer | Canopy cover measurement |
| 3 | Compass, | Navigation and showing the direction in the field |
| 4 | Suunto Clinometer | Slope measurement |
| 5 | Haga altimeter | Tree height measurement |
| 6 | Diameter tape (5m) | Tree DBH measurement |
| 7 | Linear or measuring tape (30m) | Plot layout measurement |
| 8 | Stationary (Pencil, Marker, Clipboard & Datasheet) | Field data recording and marking of measured trees in the field. |

[3] Credent technology is a Singapore based company working on aerial survey acquisition and aviation.

### 3.1.3. Software and tools

A list of software were used in this study is shown in Table 3.

Table 3. Software used in the study

| No | Software | Purpose |
|---|---|---|
| 1 | Agisoft photoscan[4] | 1. Aerial images processing<br>2. Points cloud extraction |
| 2 | ENVI accompanied with BCAL LiDAR add on[5] | DSM and DEM generation |
| 3 | eCognition Developer 8 8 | Object based image classification |
| 4 | ArcGIS version 10 | GIS analysis |
| 5 | ERDAS Imagine 2013 | Image analysis |
| 6 | Microsoft Word | Thesis writing |
| 7 | Microsoft Visio | Diagrammatic drawing |
| 8 | Microsoft Power Point | Presentation of the research |
| 9 | Microsoft Excel | Statistical analysis |
| 10 | SPSS | Statistical analysis |
| 11 | Stata | Statistical analysis |
| 12 | End note | Citation and reference |

## 3.2. Methods

The overall method consists of four major parts: field work data collection, aerial photographs processing, object based segmentation analysis and model development. Estimated camera positions were used to identify the geo-spatial location of images to a precise map known. The airborne images were processed to obtain points cloud data and further these points cloud were geo-referenced using a direct geo-referencing technique that uses estimated camera positions. The individual tree crowns delineation on the image were segmented through segmentation using eCognition software. The points cloud was processed into DSM and DTM data and to obtain the canopy height model (CHM) data. CHM data was used to produce height of the individual tree. Accuracy assessment of segmentation was implemented using goodness value approach Multiple regression was established involving CPA and height as independent variables for biomass estimation. Field data of tree parameters were used to estimate biomass of each trees and assess the accuracy of CPA, tree height derived from aerial photographs and regression model. The illustration of method is shown in Figure.5 and detailed explanations are given in the following subsection.

[4] Agisoft Photoscan is a computer vision software bundle, which image-based 3D modelling solution aimed at creating professional quality 3D content from still images (Agisoft, 2012; Geert Verhoeven, 2011)

[5] BCAL LiDAR Tools are open-source tools developed for processing, analyzing and visualizing LiDAR data by Idaho University (www.idaholidar.org).

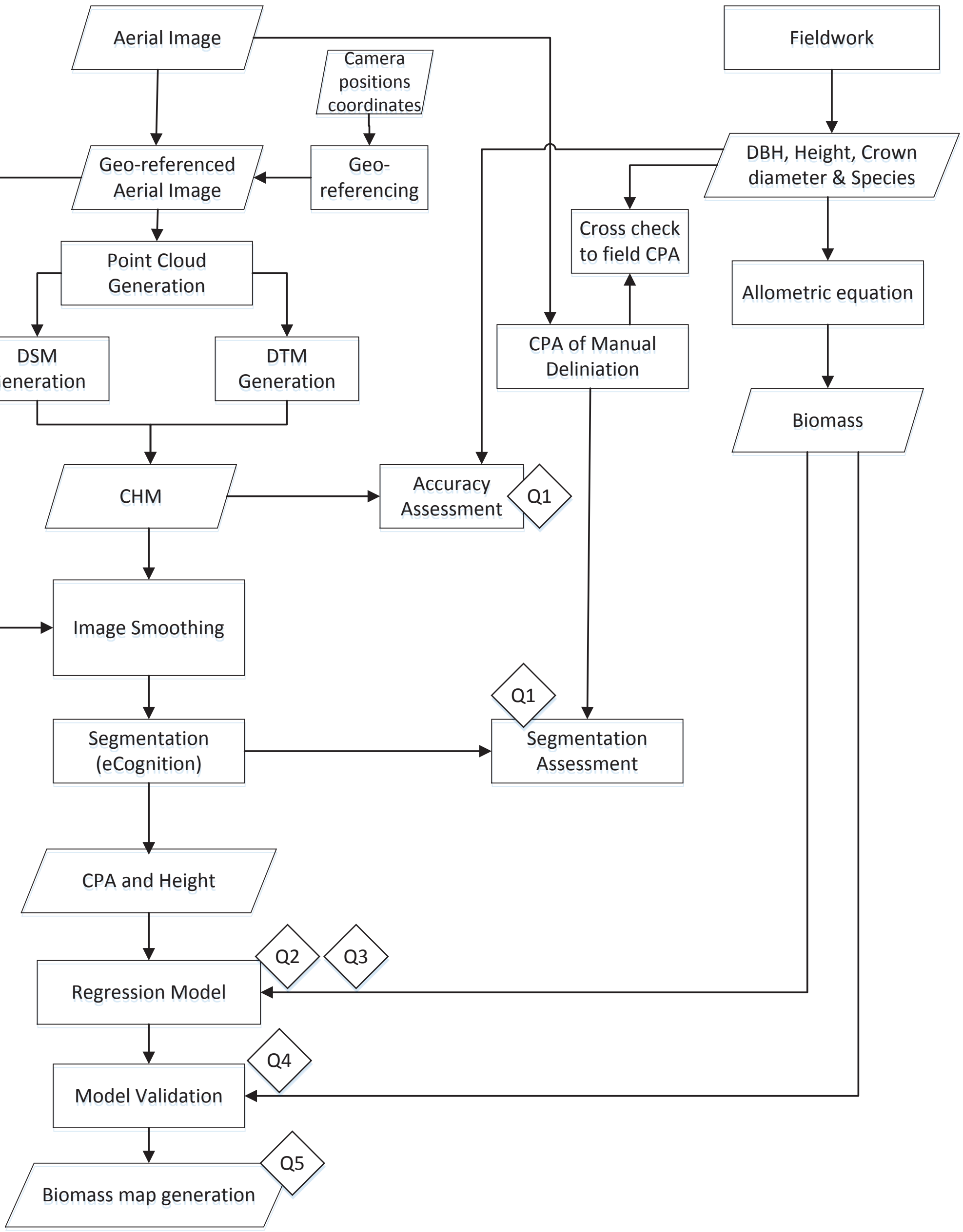


Figure 5: Flow chart of research method

#### 3.2.1. Pre-field work

The full color images that surrounding each sample plot were printed in 1: 1000 scale to make sure that trees on the image can be easily identified and recognized in the field. The shape file of the study area was created and a number of sample plots were randomly selected in ArcGIS. Subsequently, these shape files were transferred to iPAQ. The other information (road, river, elevation point and contour) were also uploaded in iPAQ in order to avoid difficulty when reaching selected plot in the field. All necessary field instruments were borrowed from ITC field equipment section for the measurement of tree parameters.

#### 3.2.2. Sampling Design

Random sampling was used to sample trees in the study area. Simple random sampling is commonly used as basic probability method. All sample units of simple random sampling has an equal probability to be selected during the selection process (Mandallaz, 2008). In this case of sample design, the entire study area is logged over area, thus there is only one stratum. The sample units of simple random sampling is generally generated without replacement, which means that there is no repetition of one sampling unit to be chosen again (Shiver & Borders, 1996).

The numbers of plots for sampling area were done using the following equations: the:

$$\boldsymbol{Area\ of\ sampling\ (a)} = \frac{\boldsymbol{sampling\ intensity\ (I)\ x\ total\ area\ (A)}}{\mathbf{100}} \qquad (Equation.1)$$

$$\boldsymbol{Number\ of\ plot\ (n)} = \frac{\boldsymbol{area\ of\ sampling\ (a)}}{\boldsymbol{area\ of\ single\ sample\ plot\ (p)}} \qquad (Equation.2)$$

Source: DOF (2004)

### 3.2.3. Plot layout

A nested circular plot was made for the measurement of tree parameters. A circular plot has less error than a square plot since the boundary is smaller in relation to the area and thus the number of trees in borderline is less (Husch et al, 2003; Lackmann, 2011). The circular plot of 500 $m^2$ with a 12.62 m radius on flat terrain was used for tree measurement. Two sub unit plots inside the main plot were also established. A medium circular sub unit plot with radius 5.64 m (100 $m^2$) and small sub unit of circular plot with radius 2.68 m (25 $m^2$); however the radius of the plots varied after applied in the field depending on the slope of terrain each plot. Slope correction table was used for plots in non-flat area.

### 3.2.4. Fieldwork

During the fieldwork, the center of each circular plot was established in the field based on the designed layout on iPAQ image. The coordinate of each center plot was recorded using iPAQ. The parameters of tree were measured in the plot such as DBH, tree height, crown cover and canopy density. Moreover, the trees in the field were identified and recognized according to printed image. After finding the sampled trees on the printed image and in the field, these trees were marked with numerical notation and recorded in the data sheet. Thus, these sampled and recognized trees were used to generate a regression model based on CPA and height. In addition, any other important information, such as slope, aspect, and exposure and unknown species were recorded.

### 3.2.5. Data analysis

After fieldwork data collection, the collected data were compiled and sorted out to identify any outliers. The field data were used to develop correlation and regression analysis and to validate the variables derived from aerial photograph. DBH and height of each tree were used for biomass allometric calculation. Moreover, CPA and height from aerial photograph were used to generate biomass estimation model in the entire study area. The field data were used to validate and assess the accuracy of model as well.

### 3.2.6. Structure from motion of computer vision techniques

Various approaches can be used to generate information in 3D image-based from 2D images. One of them is extracting point cloud through at least two overlapping images, thus a 3D image can be generated by point cloud in at least two overlapping images (Verhoeven et al., 2012). Structure from motion (SfM) is a computer vision method that is now commonly used for 3D object developing based on several overlapping images.

Structure from motion (SfM) was used to define 3D location of each object in a scene from a sequence of aerial images which is involving both their 3D structure and camera motion on its process (Ullman, 1979).

SfM determines the 3D coordinates (structure) through an analysis of the 2D motion field that is formed from the change of the camera position relative the the ground points. This method automatically extracts and identifies key-point matches between images (Lowe, 2004).

Agisoft Photoscan, computer vision software was used to extract point cloud and geo-reference the aerial images. This software has been used by Dandois and Ellis (2013) for vegetation point cloud extraction and is estimated to be ten times faster and more efficient than the other software[6]. Structure from Motion method was used to detect geometrical similarities of aerial images and monitor the movement of those points over the sequence of multiple images. This information was used to estimate the location of feature points and subsequently a three-dimensional points cloud were generated. If there are noise points, these points should be removed from point clouds using statistical outlier filtering (Sithole & Vosselman, 2004).

#### 3.2.7. Generation of 3D point cloud

The series of aerial images were processed using Agisoft Photoscan software package to generate the multispectral (red, green, blue, RGB) 3D point clouds (Figure 6). Agisoft Photoscan has option to produce point clouds with low, medium and high point densities. However, the level of required density influences the time consumption of point cloud extraction. The point cloud resulted was used to derive Digital Elevation Model (DEM), Digital Surface Model (DSM) and Canopy Height Model (CHM) as described in two following sub-sections.

Agisoft Photoscan executes several steps as part of an automated computer vision SfM to generate 3D RGB point cloud (Verhoeven, 2011). Image alignment was the first step to extract key-points of individual image and identify key-points matches among images. Accordingly, the camera position data were loaded to its correspond image, sometime the camera position is called as ground control data (Agisoft, 2012). Then, the following step was the bundle adjustment algorithm which estimated the 3D location of each point corresponds to the location and orientation of cameras (Snavely et al., 2007; Wohler, 2013). The locations of those points were estimated and a 3D point clouds was generated (Agisoft, 2012). Then, the point clouds were geo-refenced using estimated camera positions or direct geo-refencing technique which through this technique a high accuracy and consistent in object space can be obtained (Turner et al., 2012).

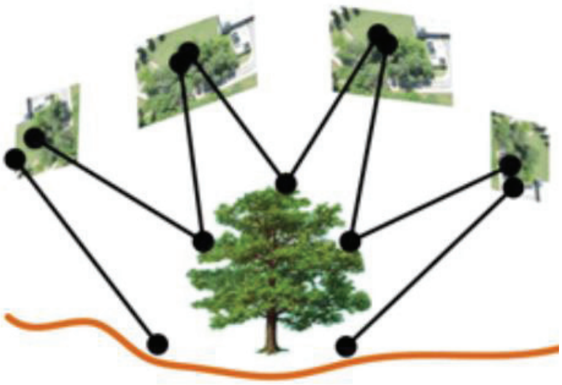

Figure 6: 3D point cloud generattion of SfM (Dandois & Ellis, 2013)

[6] In this case the researchers compared the Agisoft photoscan software to the Bundler by Noah Snavely (Dandois & Ellis, 2013).

### 3.2.8. Estimation of DTM and DSM

The point cloud resulted from Agisoft Photoscan was in *.las dataset format which is similar to the common LiDAR point cloud format. The x, y, z coordinate of aerial points cloud were processed into geographical information system through BCAL Tools software package. The point clouds were classified into ground and non-ground (vegetation) points based on elevation differences within varying windows sizes by progressive morphological filter (Zhang et al., 2003).

The classified point clouds were generated into DTM and DSM by BCAL Tools, which practically used the same procedures of LiDAR point cloud. There are several methods that can be applied to interpolate the DTM and DSM such as Inverse Weighted Distance (IWD), Universal Kriging (UK), Triangulated Irregular network (TIN), Spline interpolation and Ordinary Kriging (Childs, 2004). Nevertheless, TIN was applied to generate DTM and DSM because TIN has a simple data structure and is easily rendered by common graphic hardware .

DTM represents ground parameter of canopy height modelling and DSM denotes as vegetation elevation. DTM and DSM were generated for 1 m pixel size resolution, which the height values were represented by gray-scale values in 2D raster format.

### 3.2.9. Estimation of Canopy Height Model (CHM) of 3D Point Cloud

The CHM was generated by subtraction between DSM and DTM which resulted in the canopy height model of the individual tree (Okuda et al., 2003). Trees are considered for carbon measurement in this study, therefore all point that more than 2 meter in height were established as valid canopy height. The small vegetation were assumed less contribution to above ground biomass measurement (Mbaabu, 2012). The CHM data was also generated in 2D raster format with 1 m pixel size resolution. The CHM values were assessed by height from the field in order to validate the accuracy of aerial point cloud's CHM. The validation result was represented through their coefficient of determination ($r^2$) value.

### 3.2.10. Image Smoothening/ Filtering

Image filtering is an enhancement method which aims to improve an image visual interpretability. Through image filtering, the homogeneity of image segments can be improved and the amount of convolution of the final segmented stand boundaries can be diminished. It was expected that tree crowns with a similar shape and size to the filter could be enhanced and the noise could be reduced (Ke & Quackenbush, 2011). In this study, 3x3 low pass filtering was applied to smooth the appearance of the image. Figure 7 shows the example of 3x3 low pass filtering.

(a) Image before filtering (b) Image after filtering

Figure 7: Image filtering subset

### 3.2.11. Object Based Image Analysis (OBIA)

The basic processing units of object-oriented image analysis are segmented image objects instead of single pixels segmentation (Blaschke, 2010). Object based image segmentation analyses and subsequently classifies an object based on color, shape, texture, size and context which results in the creation of meaningful objects (Benz et al., 2004). This method relatively has higher accuracy than pixel based (Platt & Rapoza, 2008).

The image segmentation based on object oriented was carried out in eCognition software. The objects were grouped according to geographical features using scale and homogeneity parameters obtained from the spectral reflectance in the aerial image . The sequences of steps to obtain an individual tree canopy were scale parameter determination, multi-resolution segmentation, watershed transformation, morphological operation and accuracy assessment are explained in the following sub-chapters.

#### 3.2.11.1. Estimation of Scale Paramater (ESP)

The determination of appropriate segmentation in OBIA is very challenging, because there is no tool available to objectively guide the selection of suitable scales for segmentation. It needs trial and error to find the optimal scales. The degree of heterogeneity within an image object is controlled by a scale parameter by a subjective measure, in eCognition Developer 8 software it is called scale parameter. The average size of segmented image influences on the accuracy of classification. Thus, the decision of scale parameter selection is essential in remote sensing segmentation.

The ESP tool[7] aims at estimating the appropriate scales by customising the algorithm of eCognition Developer 8 for segmentation based on the concept of Local Variance (Woodcock & Strahler, 1987). Iteratively, this tool generates image objects at multiple levels in a bottom-up approach and examines the Local Variance plotted against the corresponding scale (Dragut et al., 2010).

The ESP tool was used to decide on the scale parameter of segmentation. However, series of trial and error had been also done in order to get the optimum result of segmentation. Figure 8 displays a graph of rate of change and local variance on ESP tool.

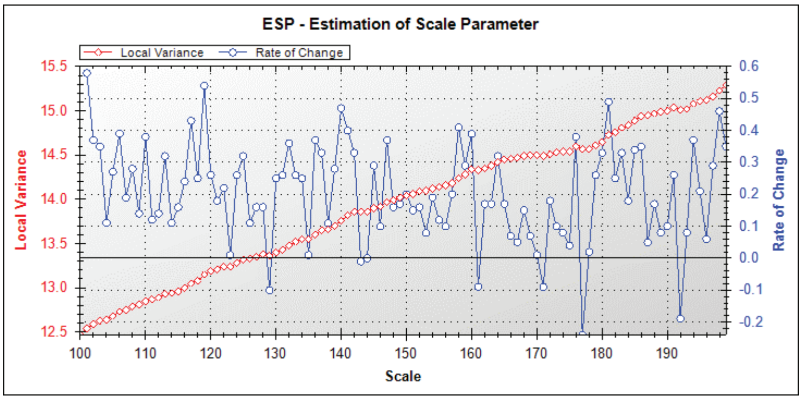


Figure 8: Tool for estimation scale parameter

[7] ESP tool was invented by Lucian Drăguţ[ab] in collaboration with Dirk Tiede[c] and Shaun R. Levick[d].
[a]Department of Geography and Geology, University of Salzburg, Salzburg, Austria; [b]Department of Geography, West University of Timis¸oara, Timis ¸oara, Romania; [c]Z_GIS, Centre for Geoinformatics, University of Salzburg, Salzburg, Austria; [d]Department of Global Ecology, Carnegie Institution, Stanford, CA, USA

#### 3.2.11.2. Multiresolution segmentation

The multi-resolution segmentation has been widely used and proven to be the one of the most successful method for image segmentation in the object-based image analysis (Baatz & Schäpe, 2000; M Kim et al., 2011; Witharana & Civco, 2014). It is embedded in the software package of eCognition Developer 8. Multi-resolution segmentation is a region based algorithm which sequentially merges pixels or existing objects (Benz et al., 2004; Trimble, 2011a). The processes of this method illustrated in Figure 9 are divided into four parts. The segmentation starts from merging single pixels in size with their neighbours, based on relative homogeneity criteria[8], into many small objects or regions. Moreover, these small objects are continuously being merged into larger regions depending on the heterogeneity among every pre-segment until the whole image has been segmented into several homogenised objects (Trimble, 2011a; Wang et al., 2013).

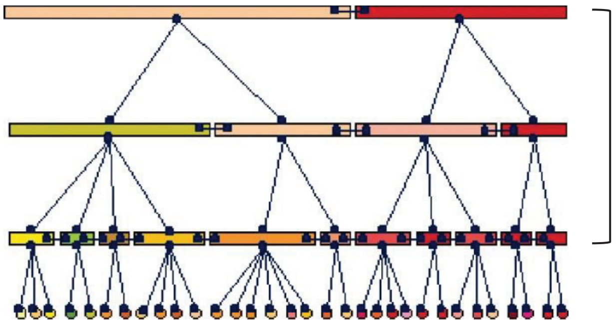


Figure 9: Illustration of multi-resolution structure in eCognition (Benz et al., 2004).

#### 3.2.11.3. Watershed

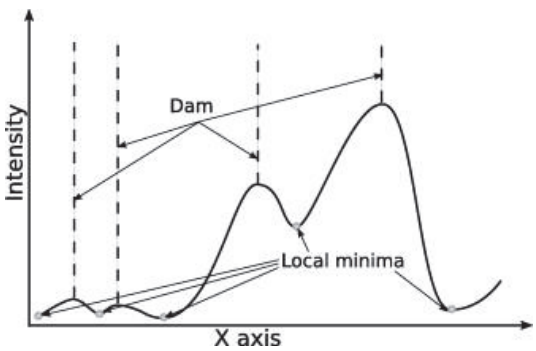


Figure 10: Illustration of watershed transformation (Derivaux et al., 2010).

The watershed transformation algorithm is usually used to separate objects in clusters into individual objects. This method is powerful technique for image segmentation (Beucher, 1992). Watershed transformation was used to separate clusters into individual tree in this study. The main idea of this method is calculating an inverted distance map based on the inverted distance for each pixel to the border of object (Trimble, 2011b), illustrated in the Figure 10. Then, the minima are flooded by increasing the level of inverted distance (dam). The dam avoids merging water (polygon) from different catchment basins. When the individual cathment basins touch each other (watershed) then the individual objects are split (Derivaux et al., 2010).

#### 3.2.11.4. Morphology

The smooting of the segmented image border was done using morphology operation. The border smoothing is based on morpholgy operations, namely the opening and closing operation. The opening

[8] The homogeneity criterion is a combination of spectral and shape criteria

operation removes pixels from an irrgular shape of image,while, the closing operation adds surrounding pixels to an image object. In this study closing morhphology was used because the smaller objects due to shadow and difference image could be filled (Trimble, 2011b).

#### 3.2.11.5. Removal of undesired objects

The tiny object with an area less than 18 pixels were removed since they had crown diameter less than 2 m which is not consider to be a tree. These groups were removed because in the dense forest small objects trigger a difficulty to identify. The objects with a high asymetry were also removed because their shape of crown is not like as a normal tree.

#### 3.2.11.6. Accuracy assessment

The validation of segmentation was done prior to develop models for aboveground biomass estimation, because the reliability of segmentation results are necessarily to be evaluated using a well defined and robust validation instrument. There are many approaches for validation of segmentation. These tools are mostly classified into three groups: which are the analytical, the empirical goodness and the empirical discrepancy groups (Zhang, 1996). The empirical goodness is commonly used for segmentation accuracy assessment (Tian & Chen, 2007). In this study the segmentation validation tool of goodness approach was applied to evaluate the segmentation results (Clinton et al., 2010). In this method, the resulted segmentations from segmentation algorithm are compared to referenced segments by human intuition (Zhang, 1996). These are the following equations to assess the segmentation results.

$$\boldsymbol{Over\ segmentation = 1 - \frac{area\ (xi \cap yj}{area\ (xi)}\ , yi \in Yi^*} \qquad (Equation. 3)$$

$$\boldsymbol{Under\ segmentation = 1 - \frac{area\ (xi \cap yj}{area\ (yi)}\ , yi \in Yi^*} \qquad (Equation. 4)$$

Where $x_i$ is the reference object and $y_j$ is the segmented object from segmentation algorithm.

The over-segmentation happens when the real condition of corresponding object is segmented into smaller sub-objects and vice versa for under-segmentation (Marpu et al., 2010). The range of over-segmentation and under segmentation is between 0 – 1. If the value of either over-segmentation or under-segmentation equals to 0, it defines as a perfect segmentation which means the segmented objects match the reference objects (Clinton et al., 2010). Therefore, using the value of unit square both over-segmentation and under-segmentation, the distance index of closeness to an ideal segmentation (D) can be calculated (Equation. 5).

$$\boldsymbol{D_{ij} = \sqrt{\frac{Oversegmentation_{ij}^2 + Undersegmentation_{ij}^2}{2}}} \qquad (Equation. 5)$$

The D value range lies between 0 – 1 and the interpretation is similar to the value of over-segmentation or under-segmentation which the D value close to 0 means close to perfect segmentation.

### 3.2.12. Above ground biomass and carbon stock calculation

The uncertainty of aboveground biomass estimation is determined by the selection of the appropriate allometric model. Several generic allometric models have been developed in tropical forest that can broadly be used for biomass estimation (Brown, 1997; Chave et al., 2005). Local allometric models for biomass estimation also exist in Indonesia which was proposed by Basuki et al. (2009), Brown (1997) and Ketterings et al (2001). However, the generic allometric model proposed by Chave et al. (2005) provides the more appropriate models in Kalimantan (Rutishauser et al., 2013)[9] which was also recommended by the IPCC guidelines in term of REDD+ (IPCC, 2006). The following equation is shown as in equation 6.

$$\boldsymbol{AGB = 0.0509\ x\ \rho D^2 H} \qquad (Equation. 6)$$

Where,

AGB : aboveground tree biomass (kg);

$\rho^{10}$ : wood specific gravity (gcm$^{-3}$);

D : tree diameter at breat height (DBH) (cm); and

H : tree height (m)

In order to convert the value of AGB to carbon stock, thus the values of AGB from that equation multiply by conversion factor (IPCC, 2007).

$$\boldsymbol{C = B\ x\ CF} \qquad (Equation. 7)$$

Where,

C : carbon stock (MgC)

B : dry biomass

CF : carbon fraction of biomass (0.47)

### 3.2.13. Regression analysis

Regression analysis is usually applied to estimate aboveground biomass. The multiple regressions have commonly been used for aboveground biomass estimation approach (Popescu, 2007). The regression analysis was carried out to model the relationship between dependent and independent variable. In this study, the segmented CPA of each tree and the height derived from 3D point clouds were considered as independent variables while the biomass of field calculation was used as a dependent variable for developing regression formula.

The evaluation of model performance is usually using the state of coefficient of determination ($R^2$) and the root mean square error. The $R^2$ explains variation of the response variable to other associated variables. Thus, the models that have high $R^2$ (close to 1 or 100%) and low RMSE indicated as a good model. The following equation was used for RMSE calculation (Equation. 8).

---

[9] This research has been done in Central Kalimantan in the old-growth secondary forest that has been selectively logged for long time and has not been clear-cut; the condition of this forest is similar to the study area. This study found that the generic model by Chave et al. (2005) was the best model with highest $R^2$ (0.964) and lowest residual standard error (0.309) and AIC (56.6). In contrast, the model developed by Basuki et al. (2009) which in the same region was greatly underestimate (Rutishauser et al., 2013).

[10] The wood specific gravities from the world agro forestry were used for species (PROSEA, 2013) that were found in the study area.

$$\boldsymbol{RMSE} = \sqrt{\frac{1}{n}\sum_{1}^{n}(\boldsymbol{Cp} - \boldsymbol{Co})^2} \qquad (Equation.8)$$

Where,
$Cp$ : predicted carbon
$Co$ : observed carbon
$n$ : number of observations

A log transform of linear regression model was established in this study to develop the aboveground regression model since the data for regression modelling shows a skewed distribution (Appendix 4.). The log transformation was done prior to model developing to correct the non-normally distributed data (Hudak et al., 2006; Zhao et al., 2012).

### 3.2.14. Aboveground biomass and carbon stock mapping

The CPA and height derived from the airborne image were used as independent variables to produce AGB and carbon stock map. These independent variables were plugged in to the regression model that was validated and thus both maps were produced to visualise the distribution of AGB and carbon stock in the study area.

# 4. RESULTS

## 4.1. Descriptives statistics of the field data

A total of 272 trees were recorded in the study area during the field data collection. The data were collected in 40 sample plots in cutting block 2010 of the PT. Karya Lestari concession. There were 30 species found in the study area. *Shorea spp* was the most dominant of tree species in the research area with occurrence of 42% followed by *Quercus spp* with 11% of occurrence. In the third place was *Dryobalanops spp* contributing 9% followed by *Syzygium spp* and *Schima wallichii* with species occurrence 8% and 5% respectively. The four least occurring species (4%) were *Eusideroxylon zwageri, Palaquium spp, Artocarpus spp and Koompassia malaccensis,* while the species with occurrence less than 1% were grouped into others (22%). A detailed of species distribution is shown in Figure 11.

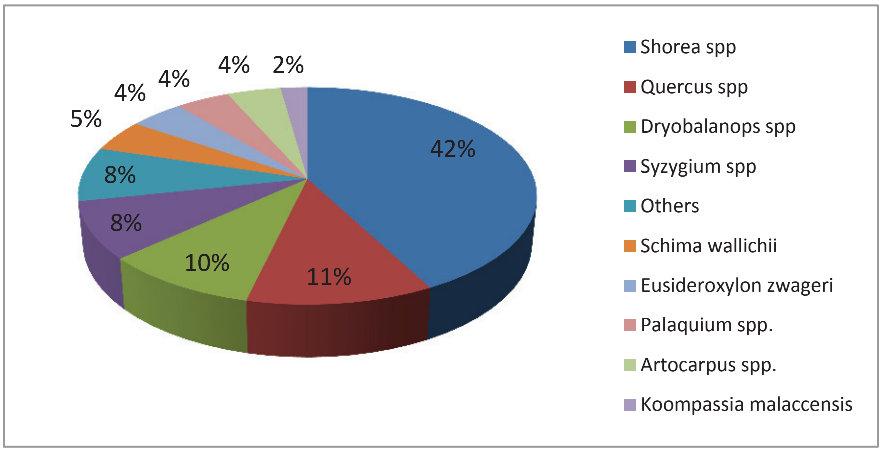


Figure 11: Species distribution

During the field work, DBH and height of the tree were also measured and analysed using box plots. Data analysis showed that *Koompassia malaccensis Maing, Dryobalanops spp,* and *Shorea spp* had the largest DBH an average, whereas *Artocarpus spp* has smallest DBH. In the same time, *Koompassia malaccensis Maing, Dryobalanops spp,* and *Shorea spp* were the species with tallest height in averagewhereas *Artocarpus spp* had the lowest height. Detailed of the average DBH and height are shown in Figure 12.

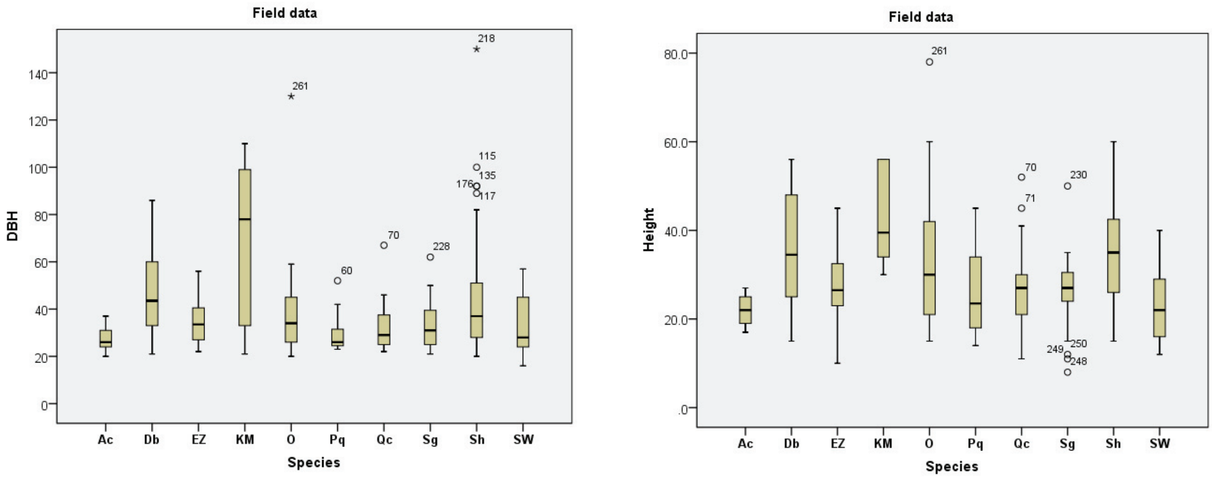


Figure 12: Box plot of the DBH and Height of species in the field

Ac=*Artocarpus spp,* Db=*Dryobalanops spp,* EZ=*Eusideroxylon zwageri T.et B*, KM=*Koompassia malaccensis Maing*, O=*Others species*, Pq=*Palaquium spp*, Qc=*Quercus spp*, Sg=*Syzygium spp*, Sh=*Shorea spp*, SW=*Schima wallichii*..

The descriptive statistics of the DBH and tree height collected from the field is shown in Table 4. The DBH has mean and median 39.62 m and 34 m respectively. Since the mean of DBH is greater than its median, it indicates that the DBH has a positive skew distribution (shown in Figure. 14). On another hand, the mean and median of height are 31.26 m and 29 m respectively. The distribution histogram of height is relatively more indicated as a normal distribution (Figure 13).

Table 4. Descriptive statistics of field data

| Attributes | Mean | Median | Std. Dev | Min | Max |
|---|---|---|---|---|---|
| DBH | 39.62 | 34 | 19.57 | 16 | 150 |
| H | 31.26 | 29 | 11.21 | 8 | 78 |

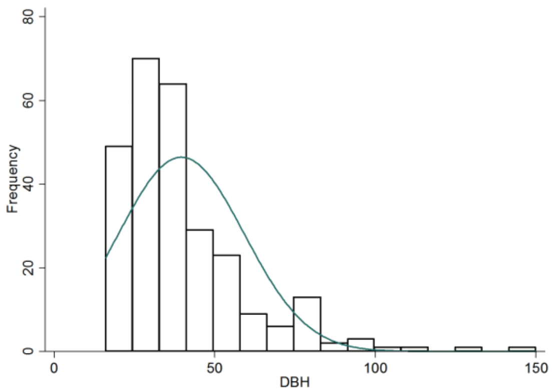


Figure 14: Distribution of DBH

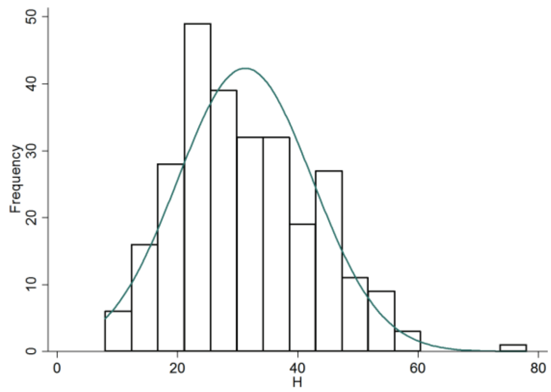


Figure 13: Distribution of field measured height

## 4.2. Points cloud generation and 3D image

Point clouds of aerial images were generated through overlapping image by structure from motion in Agisoft Photoscan. The visualisation of 3D and 2D RGB point clouds for a part of the study area is shown in the Figure 15.

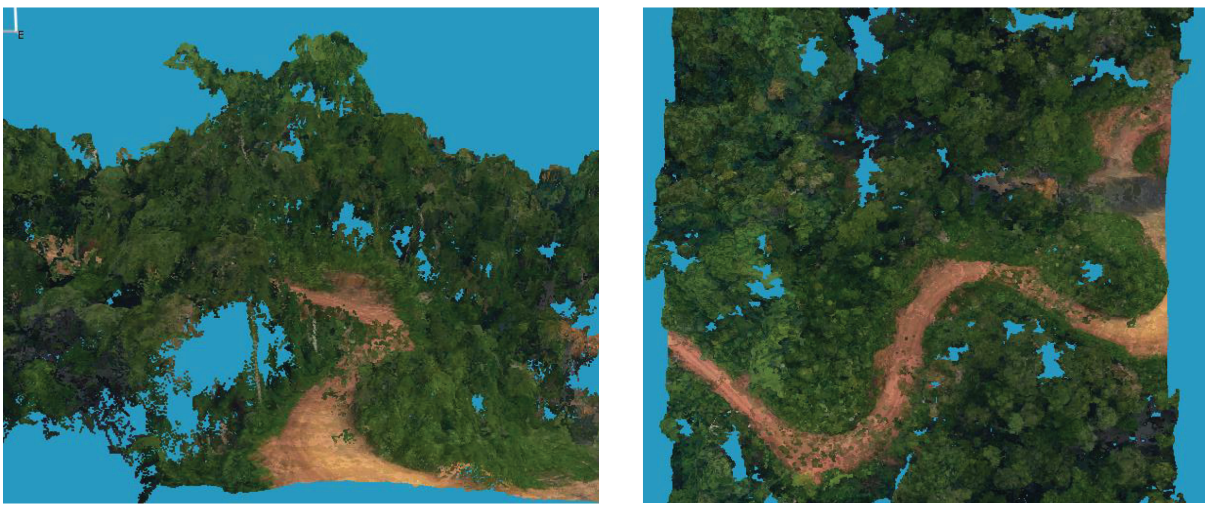

(a) 3D view

(b) 2D view

Figure 15: A subset of 3D and 2D RGB point clouds of the study area

The point clouds were extracted based on the overlapping images. In Agisoft photoscan there are options to generate point clouds of different density (low, medium and high density), in which the higher level takes the longer time and requires more computational resources. In this study the high density quality was used to generate 3D point clouds of ± 80 points per m$^2$ which has single return point cloud. The positionals error estimates obtained from image alignment were 0.83 and 1.83 for horizontal error and vertical error respectively.

## 4.3. Estimation of Canopy Height Modelling from 3D Point Cloud

The Canopy Height Model was estimated from the aerial point clouds. The CHM with 1 m of spatial resolution is a 3D surface that shows the vegetation above ground level. A representative subset of tree crown from Agisoft 3D image visualisation is shown in Figure 16.

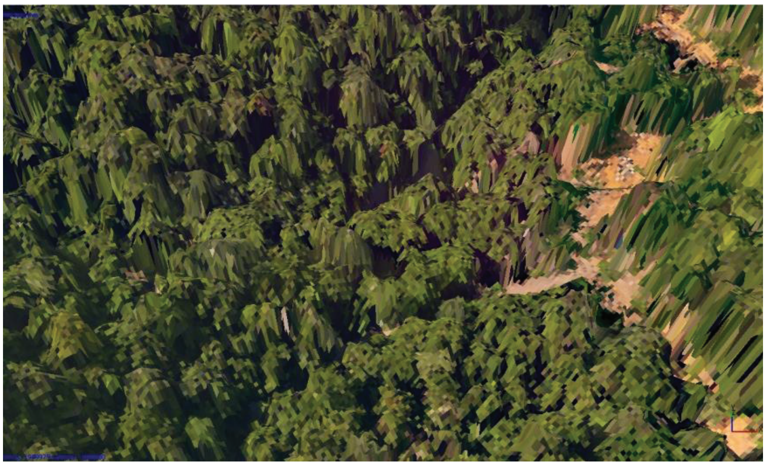

Figure 16: A subset of 3D tree crown visualisation on Agisoft

Prior to calculating the CHM, a Digital Terrain Model and Digital Surface Model were generated using 3D aerial point cloud. The subtraction of DSM from the DTM represents the absolute height of trees in the study area. The range of tree height is between 0 and 80 m, which the value of 0 means that the tree does not exist in this value as illustrated in Figure 17.

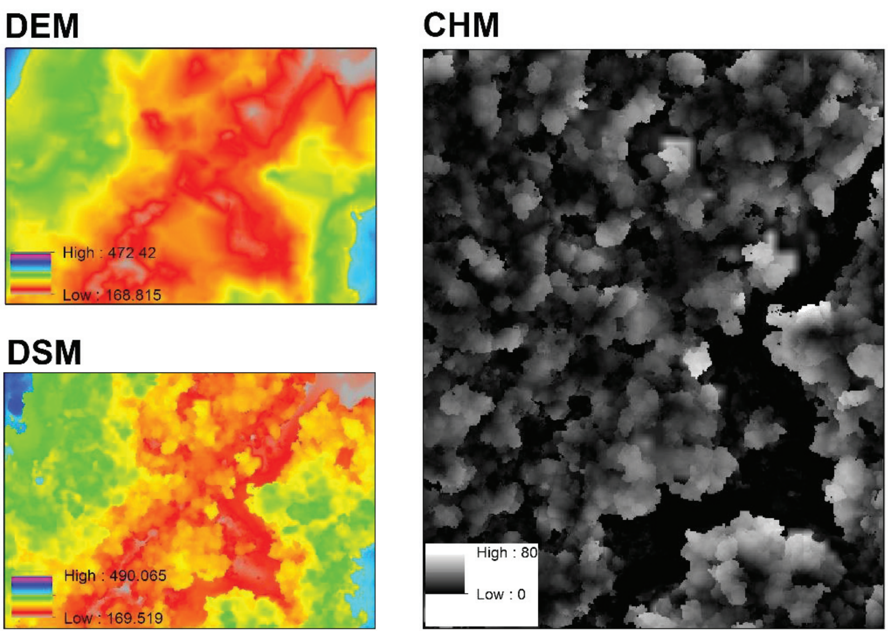


Figure 17: Illustration of DEM, DSM and CHM for a part of the study area

#### 4.3.1. CHM Validation

CHM derived from aerial point cloud was used to predict tree height in the forest. In order to validate the predicted tree height, the CHM values were examined by comparing them with the corresponding tree height measured in the field. This examination was done for 41 trees. A descriptive statistics of the field measured height and estimated CHM is shown in Table 5.

Table 5: Descriptive statistic of the field height and estimated CHM in meters

| Statistics | Field Height (m) | 3D point clouds derived height (m) |
|---|---:|---:|
| Mean | 29.97561 | 28.94133 |
| Minimum | 15 | 6.796524 |
| Maximum | 54 | 52.86322 |
| Standard deviation | 10.33317 | 9.834608 |
| Observation | 41 | 41 |

A linear regression model between CHM and tree height from field data collection was established to assess the accuracy of CHM. 3D point clouds derived height (CHM) as a dependent variable and field measured derived height as independent variable. The coefficient of determination ($R^2$) was 0.77 while the correlation value was 0.88 and RMSE was 4.9 (Figure.18). There was an indication that height derived from 3D point clouds was under estimated by 1.03 m on average compared to height derived from field.

**Scatter plot**

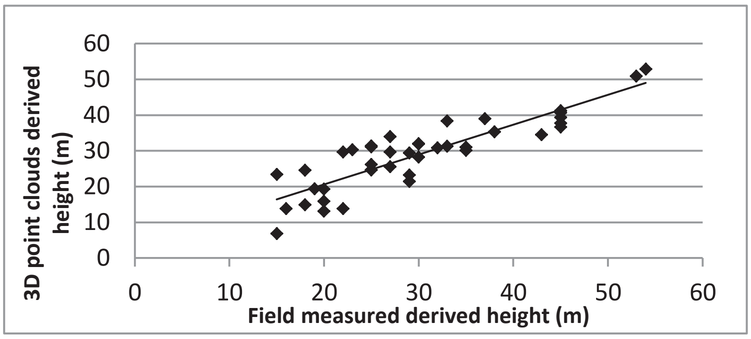


**Summary of fit**

| | |
|---|---:|
| Correlation coefficient | 0.88 |
| R Square | 0.77 |
| Adjusted R Square | 0.681 |
| RMSE % | 16.60 |
| Intercept | 3.2243 |
| Slope | 0.9243 |
| Observation | 41 |

Figure 18: Scatter plot of relationship and summary of fit between height field from field and estimated height from 3D aerial point cloud

The relationship test between height measured in the field and estimated height from 3D aerial point cloud were also assessed using a paired t-test. Since the t-calculated was greater than t-critical, the relationship was stated statistically significant at confident level 95% (Table.6).

Table 6: Paired t test between height from field and estimated height from 3D aerial point clouds

| Variable | Obs | Mean | Std. Err. | Std. Dev. | [95% Conf. | Interval] |
|---|---|---|---|---|---|---|
| H | 41 | 29.97561 | 1.61377 | 10.33317 | 26.71406 | 33.23716 |
| CHM | 41 | 28.94133 | 1.535908 | 9.834608 | 25.83714 | 32.04551 |
| diff | 41 | 1.03428 | .776056 | 4.969183 | -.5341875 | 2.602748 |

```
    mean(diff) = mean(H - CHM)                              t =   1.3327
Ho: mean(diff) = 0                         degrees of freedom =       40

Ha: mean(diff) < 0           Ha: mean(diff) != 0           Ha: mean(diff) > 0
Pr(T < t) = 0.9049       Pr(|T| > |t|) = 0.1902            Pr(T > t) = 0.0951
```

## 4.4. Image Segmentation

Image segmentation was carried out on aerial image using multi-resolution segmentation embedded in eCognition Developer 8. This method was applied to group neighbouring pixels into homogenous objects based on their homogeneity.

### 4.4.1. Estimation of Scale Parameter (ESP)

In order to find the most apropriate scale for multi resolution parameter, the ESP tool was used to decide on the scale parameter of segmentation. The peaks that are shown in the ROC-LV graph indicates the image could appropiately be segmented at which level. Figure 19 shows the estimation of scale paramater for aerial image of study area which at scale parameter 119 or 125 were the apropriate scale parameters.

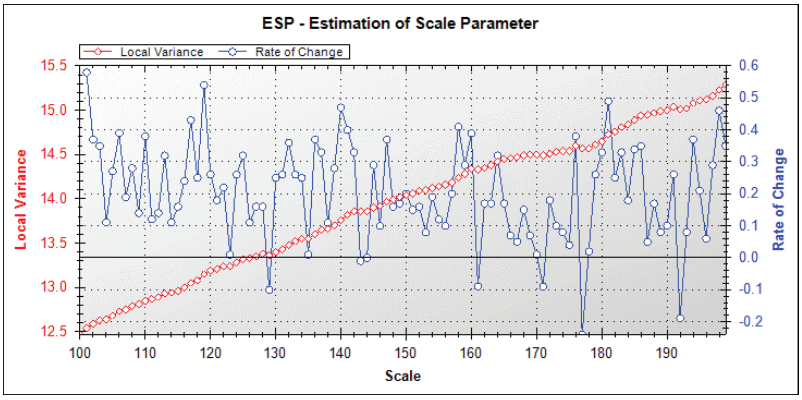


Figure 19: ESP Tool of Aerial Orthophoto

### 4.4.2. Multi resolution segmentation

The multi-resolution method was carried out using scales parameter showed as peaks on the ROC curve (Figure 19). The scale parameter of 119 and 125 were evaluated to determine appropriate scale parameter. As a result, the larger scale level tends to segment objects on image which has wider size of segmented area compare to the smaller level. Figure 20 illustrates the results of both scale levels. The differences of segmentation result are shown by blue circles for scale parameter 119 and red circles for scale parameter 125.

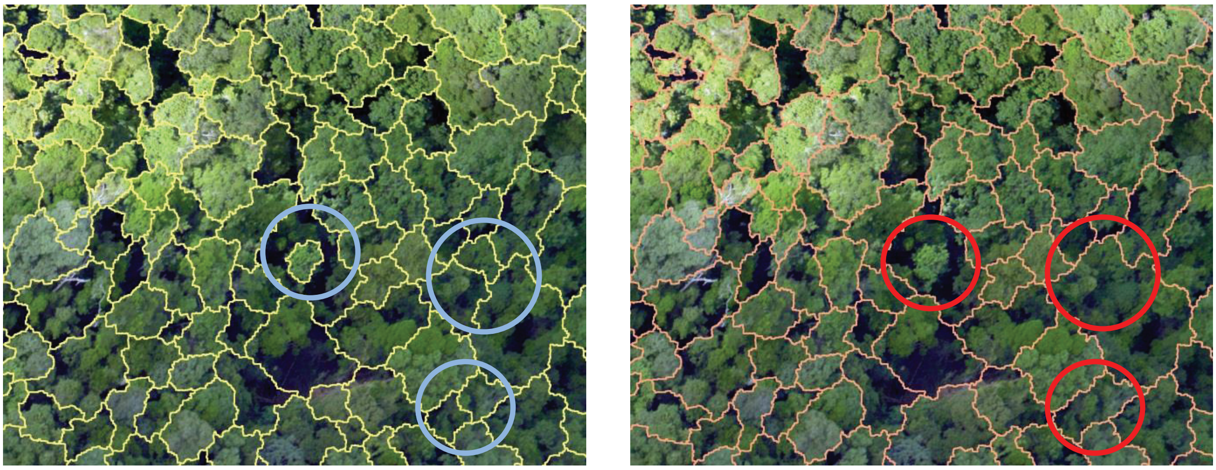

(a). Scale Parameter 119 (b). Scale Parameter 125

Figure 20: Representation of scale parameter 119 and 125

#### 4.4.3. Accuracy of segmentation

The D value was assesed to evaluate the accuracy of segmentation of each scale level. The scale parameter of 119 was applied on multi-reslution segmentation which was over segmented by 0.38 and under segmented by 0.41. At the same time, the over segmentaion value of the scale parameter of 125 was 2.25 and the under segmentation value was 0.40. Therefore, the D value of the scale parameter of 119 and 125 were 0.36 and 0.58 respectively. This value indicates that the scale level of 119 is more appropriate than the scale level of 125 which its D value is closer to 0 (Table 7).

Table 7: D Value of Scale parameter

| Scale Parameter | ∑OS | ∑US | $OS^2$ | $US^2$ | D-Value |
|---|---|---|---|---|---|
| 119 | 1.39 | 0.57 | 0.21 | 0.06 | 0.36 |
| 125 | 2.25 | 0.40 | 0.64 | 0.04 | 0.58 |

OS: Over segmentation; US: under segmentation; SP: Scale parameter

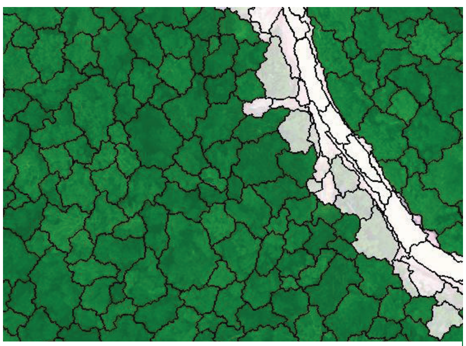

Figure 21: A subset of segmentation result using scale parameter 119

Thus, the multi-resolution segmentation was done using scale parameter 119. Figure 21 shows a subset of segmented object using scale parameter 119.

## 4.5. Model Development and Validation

### 4.5.1. Relationship among variables

Prior to developing a model for aboveground biomass measurement, the strength of relationship among variables was evaluated. In Figures 22, 23, 24 and 25 show that the correlation between DBH-H from field, DBH-CPA and DBH-Height from 3D point clouds were less than 0.60. The corresponding values of $R^2$ were 0.31, 0.02 and 0.34 respectively.

**Scatter plot**

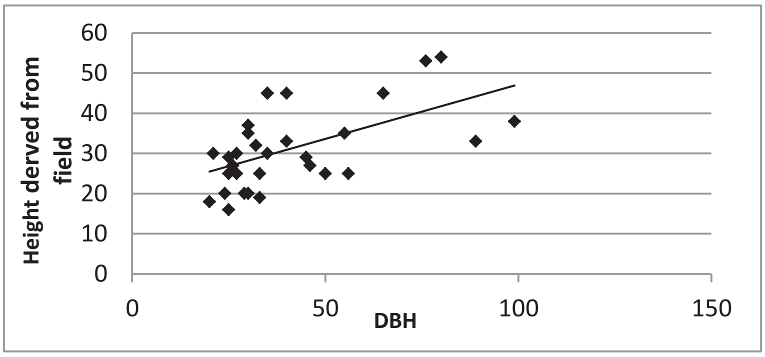


**Summary of fit**

| | |
|---|---|
| Correlation coefficient | 0.5578 |
| R Square | 0.3112 |
| Adjusted R Square | 0.2874 |
| RMSE % | 42.25 |
| Intercept | 5.501 |
| Slope | 1.147 |
| Observation | 31 |

Figure 22: Relationship between DBH and height derived from field

**Scatter plot**

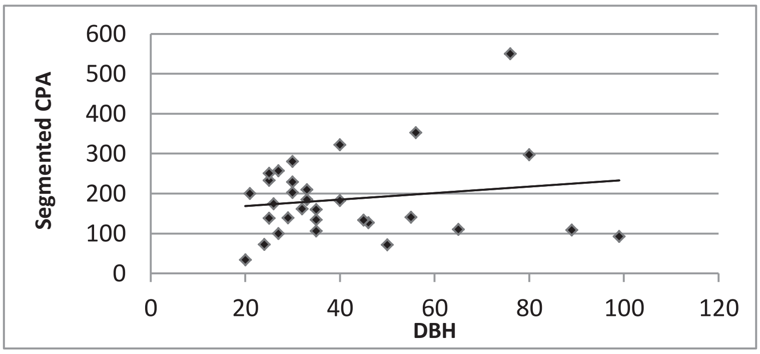


**Summary of fit**

| | |
|---|---|
| Correlation coefficient | 0.1633 |
| R Square | 0.0267 |
| Adjusted R Square | 0.0069 |
| RMSE % | 50.22 |
| Intercept | 35.246 |
| Slope | 0.033 |
| Observation | 31 |

Figure 23: Relationship between DBH and segmented CPA from multi-resolution segmentation

**Scatter plot**

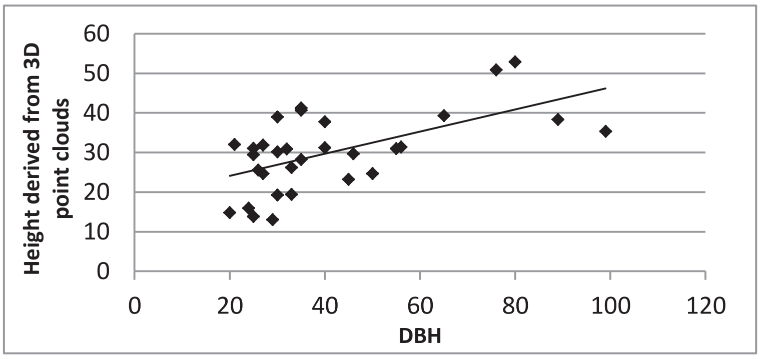


**Summary of fit**

| | |
|---|---|
| Correlation coefficient | 0.5899 |
| R Square | 0.3480 |
| Adjusted R Square | 0.3255 |
| RMSE % | 41.09 |
| Intercept | 3.938 |
| Slope | 1.246 |
| Observation | 31 |

Figure 24: Relationship between DBH and height derived from 3D point clouds (CHM)

| Scatter plot | Summary of fit | |
|---|---|---|
| 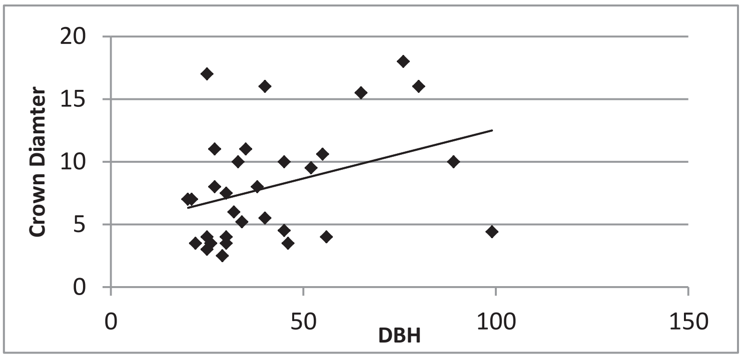 | Correlation coefficient | 0.3523 |
| | R Square | 0.1241 |
| | Adjusted R Square | 0.0939 |
| | RMSE % | 47.69 |
| | Intercept | 29.062 |
| | Slope | 1.5893 |
| | Observation | 31 |



Figure 25: Relationship between crown diameters derived from field and DBH

#### 4.5.2. Correlation analysis among variables used for regression analysis

The Pearson's correlation among variables used for model development was established to evaluate the strength of the relationship between field measured diameter breast height DBH, height derived from point cloud (written as CHM) and above ground biomass (AGB). The relationship among variables is shown in Table 8.

Table 8: Correlation among variables of regression model

| Variables | df (n-2) | r | R square | P value |
|---|---|---|---|---|
| DBH and AGB | 29 | 0.961 | 0.924 | 0.000 |
| CHM and AGB | 29 | 0.660 | 0.435 | 0.000 |
| CPA and AGB | 29 | 0.210 | 0.044 | 0.257 |

There is a strong positive correlation between DBH and above ground biomass. The correlation of variables extracted from 3D images shows that the correlation coefficient between CHM and AGB is higher than correlation coefficient between the CPA and AGB. It indicates that above ground biomass is more strongly correlated to the height derived from point cloud than to the crown projection area.

#### 4.5.3. Model development

##### 4.5.3.1. Descriptive statistic of variables used for modelling

A total of 31 mixed trees of various species were used to develop aboveground biomass model. These trees correspond to the total number of correctly classified and matched with segmented CPA. Table 9 shows the descriptive statistics of variables used for biomass modelling.

Table 9: Descriptive statistics of the variables were used for regression modelling.

| | Variable | | |
|---|---|---|---|
| | CHM | CPA | AGB |
| Mean | 30.05745 | 185.991 | 3542.576 |
| Standard deviation | 9.806446 | 102.4274 | 4338.091 |
| Minimum | 13.01447 | 34.36492 | 432.65 |
| Maximum | 52.86322 | 550.6546 | 16303.1 |
| Observations | | 31 | |

The normality test was used to assess the dependent variables before developing a model for aboveground biomass measurement. The skewness value of CPA was 0.0009 that is significantly different from a normal distribution at the 5% significant level, thus this variable was not normally distributed (Appendix 4). Meanwhile, the kurtosis value of CPA also indicated that the observations are not normally distributed.

Multiple regressions using natural logarithmic transformation were carried out to analyse the relationship between aboveground biomass and the tree variables which were extracted from high resolution 3D images. The log transformation was done to help fit the variables into the model that makes the distribution more normal.

The multiplicative model in log transformed is shown in Equation 9. In order to calculate estimated aboveground biomass, the resulted value of biomass through the model was transformed into anti log value.

$$ln\hat{Y} = \beta_0 + \beta_1 lnX_1 + \beta_2 X_2 \ldots\ldots\ldots\ldots\ldots\ldots\ldots\ldots\ldots\ldots\ldots\ldots\ldots\ldots . Equation\ 9$$

$\hat{Y}$ : Predicted aboveground biomass from allometric equation
$X_1$ : Height derived from 3D point clouds
$X_2$ : Crown Projection Area derived from automated segmentation
$\beta_1$ : Intercept
$\beta_1$ and $\beta_2$: Coefficients of $X_1$ and $X_2$

Multiple liner regression model was established for aboveground biomass estimation. A total of 31 observations were involved in the model development. The $R^2$ of the model was 0.5666 while the adjusted $R^2$ was 0.5356. The model developed for aboveground biomass estimation in study area is shown below (equation 10).

$$lnAGB = 1.29 + 2.34lnCHM - 0.30CPA \ldots\ldots\ldots\ldots\ldots\ldots\ldots\ldots equation\ 10$$

Accordingly, an F – test was applied to evaluate the significance of the model. The results in Table 10 shows that F calculated is 18.30 or greater than F from critical table that is 3.34 at 95% confident level, thus dependent variable can statistically be significant explained by the independent variables.

Table 10: Regression analysis of lnAGB, LnCHM and lnCPA

| Source | SS | df | MS |
|---|---|---|---|
| Model | 18.0764863 | 2 | 9.03824317 |
| Residual | 13.8295671 | 28 | .493913111 |
| Total | 31.9060535 | 30 | 1.06353512 |

| | |
|---|---|
| Number of obs | = 31 |
| F( 2, 28) | = 18.30 |
| Prob > F | = 0.0000 |
| R-squared | = 0.5666 |
| Adj R-squared | = 0.5356 |
| Root MSE | = .70279 |

| lnAGB_field | Coef. | Std. Err. | t | P>\|t\| | [95% Conf. | Interval] |
|---|---|---|---|---|---|---|
| lnCHM | 2.346047 | .4004382 | 5.86 | 0.000 | 1.525786 | 3.166307 |
| lnCPA | -.3004905 | .2591449 | -1.16 | 0.256 | -.8313248 | .2303438 |
| _cons | 1.292424 | 1.42466 | 0.91 | 0.372 | -1.62586 | 4.210708 |

#### 4.5.4. Model Validation

The model was validated against field data using 10 observations. The coefficient of determination between predicted AGB and observed AGB was 0.59. This shows that around 59.96% of the observed carbon in the study area was explained by the model. The RMSE for the validated observation was 33%. Figure 26 shows a detail of model validation.

**Scatter plot**

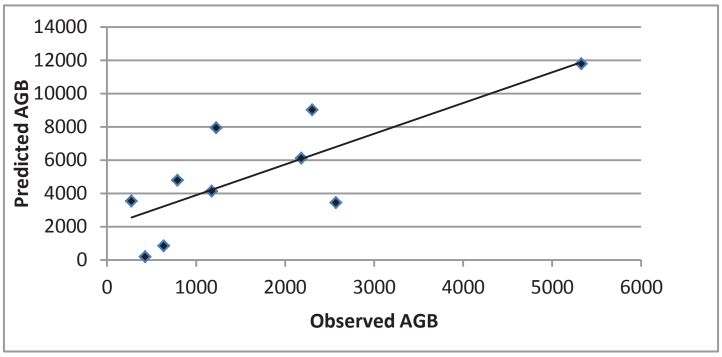


**Summary of fit**

| | |
|---|---|
| Correlation coefficient | 0.7743 |
| R Square | 0.5996 |
| Adjusted R Square | 0.5495 |
| RMSE | 1015.8 |
| RMSE % | 33.02 |
| Intercept | 16.1367 |
| Slope | 0.3242 |
| Observation | 10 |

Figure 26: Model validation

### 4.6. Aboveground biomass and carbon Mapping

The validated model was applied to estimate the amount of aboveground biomass and carbon in the study area. The transformed value of biomass was converted into carbon by multiplying the biomass value by 0.47. The above ground biomass map of the study area is shown in Figure 27.

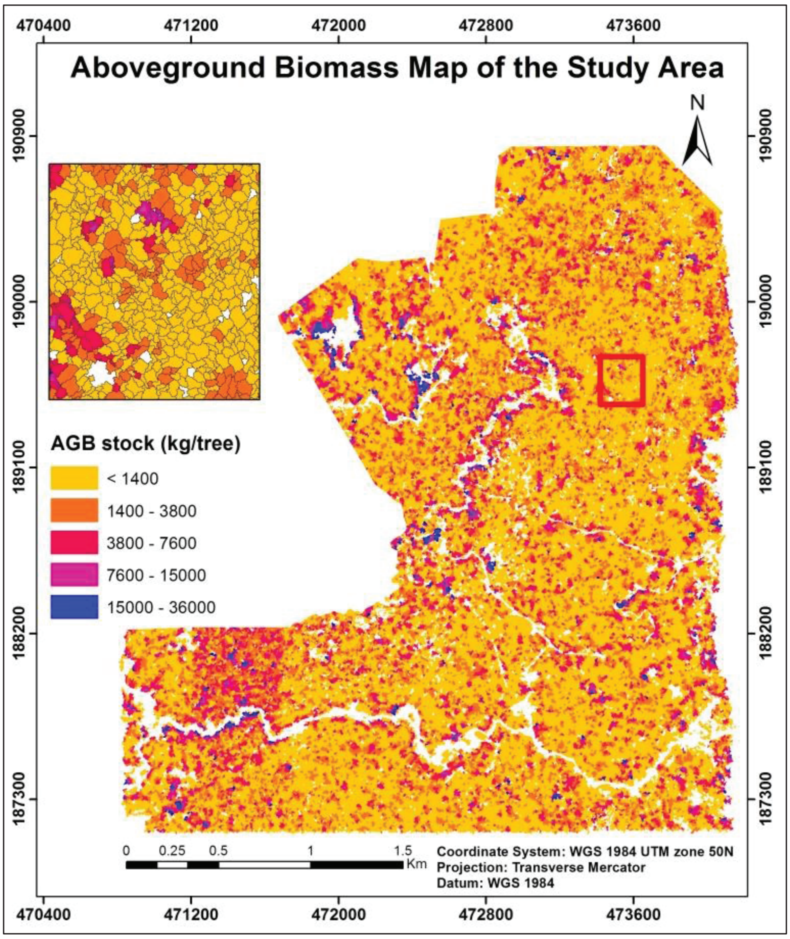


Figure 28: Above ground biomass map of the study area

Thus, the aboveground biomass was converted into carbon stock using conversion that 1 unit of aboveground biomass equals to 47% unit of carbon. Figure 28 shows carbon stock map of the study area.

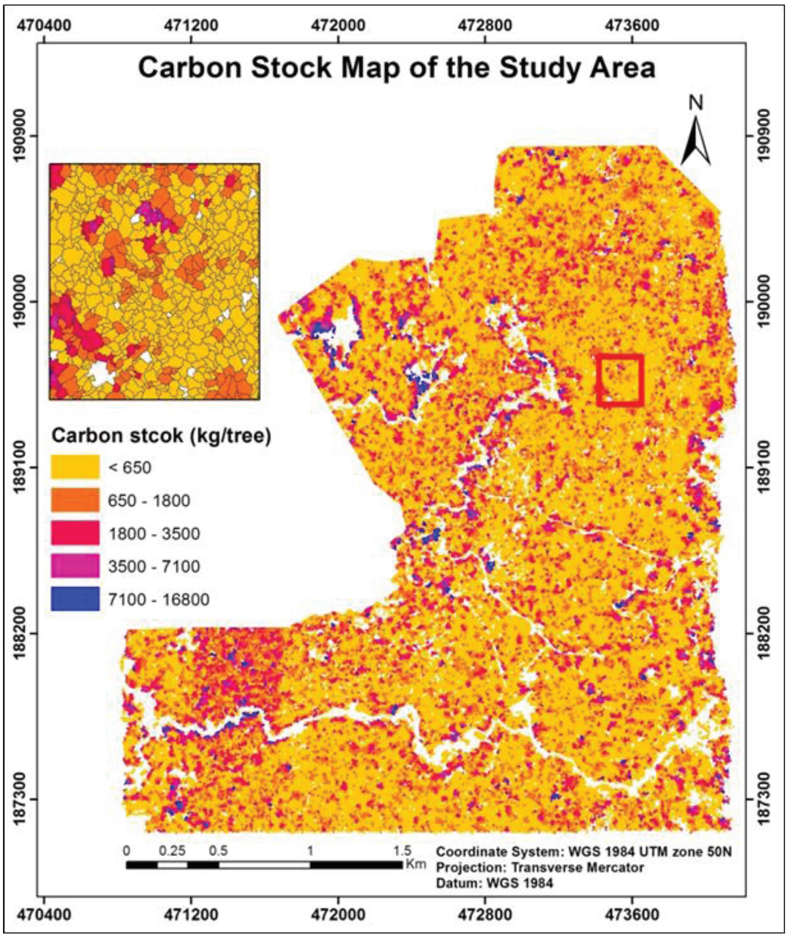


Figure 29: Carbon stock map of the study area

The total biomass in the study area was around 146,810 MgC and total carbon was about 69,000 MgC. The study area approximately covers 770.63 ha, thus the biomass per hectare was 190 $MgCha^{-1}$ and carbon was 89 $MgCha^{-1}$. The total amount of carbon in each sample plot was also estimated on average base in which each plot has 32.21 ton of above ground biomass and the total carbon each plot was 15.14 ton. Aboveground biomass and carbon stock estimation is presented in Table 11.

Table 11: Aboveground biomass and carbon stock estimation of in the study area

| Average Biomass per plot (Kg) | Average Biomass per ha (Mg) | Average Carbon per plot (Kg) | Average Carbon per ha (Mg) | Total Biomass (Mg) | Total Carbon (Mg) |
|---|---|---|---|---|---|
| 32,205.82 | 190.51 | 15,136.74 | 89.54 | 146,810.04 | 69,000.72 |

### 4.7. An alternative model of biomass estimation

Since, the modelling of biomass  involving biomass, CPA and Height derived from point clouds was not quite satisfactory, an alternative model was developed. A multiple regression that involved lnAGB as the independent variable and with lnDBH and lnCHm as dependent variables was evaluated. The coefficient of determination of this model was 0.97. Thus, the estimated biomass could be explained by 97% using this model. The RMSE value of this model was 0.17. The F test shows that F calculated (534.54) is greater than F table (3.34), thus the model is statistically significant at 95% significant level. Table 12 shows the details of the regression analysis assessment. This model shows a stronger relationship compared to the model of AGB using both CPA and CHM derived from 3D point cloud. The model developed  using AGB against CHM derived from 3D point cloud and CPA indicates a low relationship according to its value of $R^2$.

Table 12: Regression Analysis of lnAGB with lnDBH and lnCHM

| Source | SS | df | MS | | |
|---|---|---|---|---|---|
| | | | | Number of obs = | 31 |
| | | | | F( 2, 28) = | 534.54 |
| Model | 31.09174 | 2 | 15.54587 | Prob > F = | 0.0000 |
| Residual | .81431341 | 28 | .029082622 | R-squared = | 0.9745 |
| | | | | Adj R-squared = | 0.9727 |
| Total | 31.9060535 | 30 | 1.06353512 | Root MSE = | .17054 |

| lnAGB_field | Coef. | Std. Err. | t | P>\|t\| | [95% Conf. | Interval] |
|---|---|---|---|---|---|---|
| lnDBH | 1.911612 | .0881422 | 21.69 | 0.000 | 1.731061 | 2.092164 |
| lnCHM | .8065939 | .1072817 | 7.52 | 0.000 | .5868374 | 1.02635 |
| _cons | -2.012936 | .3159164 | -6.37 | 0.000 | -2.660061 | -1.36581 |

#### 4.7.1. Model validation of an alternative approach

The alternative model validation shows that the $R^2$ value between predicted AGB and observed AGB was 0.96 which is  higher than the previous model. It shows that around 96% of the observed carbon in study area was explained by the model. The RMSE for the validated observation was 16%. A detail of model validation of an alternative approach is shown in Figure 29.

**Scatter plot**

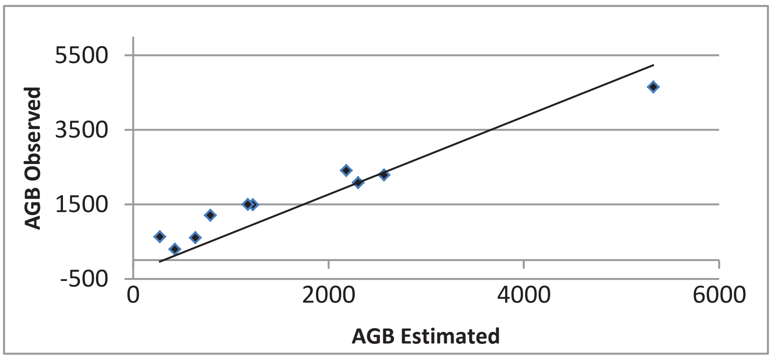


**Summary of fit**

| | |
|---|---|
| Correlation coefficient | 0.9840 |
| R Square | 0.9683 |
| Adjusted R Square | 0.9644 |
| RMSE | 285.61 |
| RMSE % | 16.88% |
| Intercept | -327.9291 |
| Slope | 1.1800 |
| Observation | 10 |

Figure 29: Model validation of an alternative model

# 5. DISCUSSION

## 5.1. Field data collection

In this study the species found in the field was dominated by family of Dipterocarpaceae that as typical of Borneo forest (Slik et al., 2002). Interestingly, The largest DBH and the highest tree was *Koompassia malaccensis Maing* (local name is Bangris) because the concession company do not cut this species of tree. There is an unwritten law that the company is not allowed to cut this tree or will be fined by local community *(Dayak etnic)* in the surrounding forest, because there is honeycomb on this tree has an economics values for local people[11]. The shortest species was *Artocarpus spp* that in the field measurement the height ranging from 17 – 27 m. As a typical of *Artocarpus spp*, its height is ranging from 8 m to 25 m (Elevitch & Manner, 2006). The distribution of DBH showed as a positive skew because the DBH of trees from field data were mostly less than 50 cm and only few trees have DBH more than 50 cm. The study area was a logged over area, thus the commercial trees that have DBH higher than 50 cm have been felled down by timber company as ruled by Indonesian selective logging (TPTI).

## 5.2. 3D point clouds

3D point clouds were generated using the overlap of aerial images. The point clouds are only able to observe the location that can be seen in the multiple images. The understory areas could not be observed because they are blocked by the over-story. However, LiDAR data offers comprehensive measured observations, from top of tree crown to the ground (Dubayah & Drake, 2000). The density of point clouds of this study was ±80 $m^{-2}$ with the positions estimated errors were horizontal: 0.83 m and vertical: 1.83 m. According to Clark et al. (2004) the accuracies that generally considered acceptable for most forestry applications are ranging from one to four meter. This mean that the resulted generated point clouds from airborne images is reasonably accurate. The point cloud resulted in this study only has single return that might impeed the accuracy of digital terrain model (DTM) generation. On another hand, LiDAR data are able to capture multiple returns and to reach the ground level, even in forested areas which makes possible the generation a high accuracy of DTM (Lisein et al., 2013). However, as an advantage, the density of aerial point cloud significantly quite higher than LiDAR data (Leberl et al., 2010).

## 5.3. CHM

Canopy height model (CHM) derived from 3D point clouds was described in this study. Around 63% of CHM was underestimated and 37% was overestimated compared to measured height in the field. Consequently, the overall CHM was underestimated relative to field measured height by around 1.03 m on average. The value of determination was 0.77. The RMSE for predicted CHM was 4.97 with RMSE percent 16.60%. The paired t-test also confirmed that the relationship between height measured in the field and height estimated from the point clouds derived from 3D Aerial images is statistically significant at confident level 95%.

Several researchers who have estimated tree height using 3D point cloud of aerial image came up with different results. The tree height (CHM) estimated using point clouds in the temperate deciduous forest

[11] This information was based on the author observation during data collection in the study area.

was reported having high value of coefficient of determination and consequently correlated to height measured in the field with $R^2$ ranging from 0.63 to 0.84 with the leaf-on condition (Dandois & Ellis, 2013). Nurminen et al. (2013) conducted a study in pine forest during leaf-on condition in autumn and obtained 0.97 of the $R^2$ value. Using LiDAR data, Kwak et al. (2007) found the coefficient of determinations ranging from 0.77 to 0.80 for height estimation in coniferous forests and 0.74 for height estimation in broad leaf forest.

The coefficient of determination found in this study is in the range of the values found in the study conducted by Dandois and Ellis (2013) and comparable to tree height estimation using LiDAR data. However, the value of $R^2$ in this study is lower than $R^2$ value obtained by Nurminen et al. (2013). The previous studies were carried out in a low density coniferous forest. Therefore the conditions were different to those of our study in the tropical rain forest. Low density forests have a large number of tkey-points matches that can be captured by 3D camera view-points (Lowe, 2004). The coniferous forest also has more conical crown shape than in broadleaf forest where crowns are more rounded (Ke & Quackenbush, 2008). Thus, the key-points matches of individual tree in low density forest can be more than in the dense forest condition (e.g., tropical forest) and consequently the estimated tree height can be precisely derived. Figure 28 illustrates the differences of aerial images captured in coniferous temperate forest and tropical rain forest.

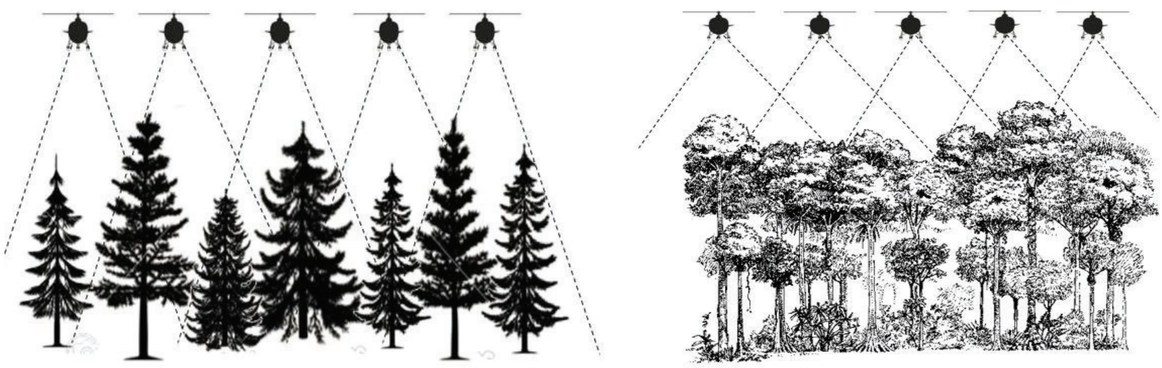

(a). Coniferous forest (b). Tropical rain forest

*Source: http://www.mediahex.com/Stratification_(ecosystem)*

Figure 30: The condition in coniferous forest (a) and tropical rain forest (b)

A 3D aerial point cloud is promising for canopy height model estimation and comparatively similar to LiDAR data. However the result of the CHM estimated can be improved using a combination of the airborne point clouds with LiDAR data. Several studies revealed that the 3D aerial point cloud combined with LiDAR DTM or with high resolution of DTM increased the estimation accuracy of the absolute height of object compared to the usage of aerial point clouds stand-alone (Dandois & Ellis, 2010; Moreira, 2013). The reason behind this, is the point clouds of aerial image have one return which cannot estimate the ground level of terrain properly. Moreover, the filtering of ground points was more problematic in the dense forest using aerial point clouds. These issues generated a problem in the DTM interpolation process because of the lack of reliable ground elevation. Because of this, the produced DTM was with low accuracy. On another hand, LiDAR data have multiple returns are able to generate a highly accurate ground level or digital terrain model . The low quality of DTM generated from aerial point clouds is one of the reasons for underestimation of canopy height model CHM because the DSM of aerial point clouds were not subtracted from high accurately DTM as a DTM produced from LiDAR. Another possible reason that the filtering for ground points was more difficult in the dense forest using aerial point clouds, since the aerial point clouds only have one return. Thus, this issue caused the accuracy of DTM interpolation to be relatively low.

### 5.4. Image segmentation and accuracy assessment

The image segmentation was done using multi-resolution segmentation method that was described in section 3.2.11 and the result is presented in section 4.4

Because multi-resolution segmentation accompanied with watershed transformation is positively able to segment highly heterogeneous forest tree crowns (Kim et al., 2008), this method was selected for automatic delineation rather than the alternative approach of individual tree crown segmentation. The alternative method of individual tree segmentation takes the tree top into consideration. In other words, the highest value of brightness is identified as the top of tree (Tiede et al., 2006; Wang et al., 2004). This method is usually applied in the conical shaped vegetation where only one tree top of each individual tree is possible (Ke & Quackenbush, 2008). The area of this study is a natural tropical rain forest which consists of different canopy level, different age and different species of vegetation. In the tropical rain forests, it is possible to have more than one tree tops within one canopy of each tree compared to coniferous forest (illustrated in Figure 31). Since this research is dealing with tropical rain forest with the chance of multi-tops tree, the multi-resolution segmentation was performed to address the complexity of tropical forest segmentation, instead of tree top approach. Lamonaca (2008) proved that the multi-resolution segmentation is a robust technique to segment spatially structured heterogeneous forest and to derive the meaningful information of forest structural attributes. Figure 31 shows the complexity of the structure of the tropical rain forest similar to our study area.

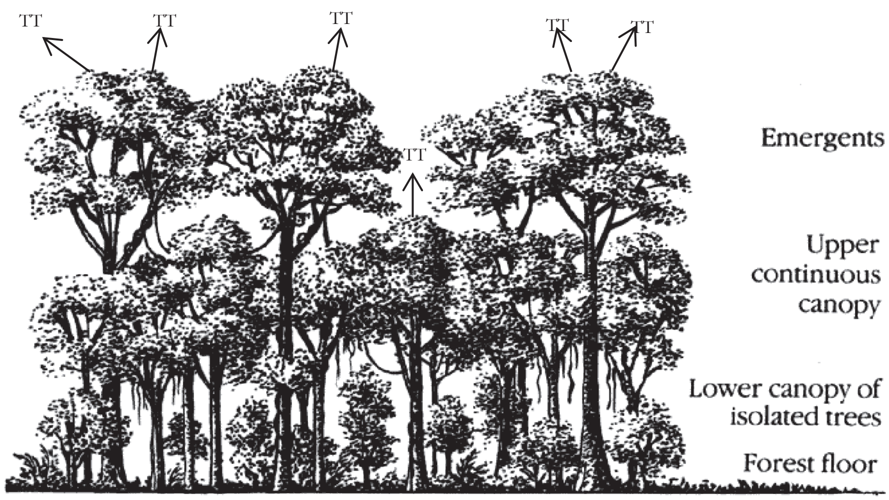


Figure 31: Canopy layers in tropical rain forest (TT: Tree top)
*Source: http://www.sivatherium.narod.ru/library/Dixon_2/02_en.htm*

The closeness accuracy was used to assess the results of the multi-resolution approach (Clinton et al., 2010) in this research. The accuracy result obtained in this research was 64% with D value 0.36. This result was lower than that of Wang et al. (2004) and (Kwak et al., 2007) whom obtained 75.6% and 86% respectively of segmentation accuracy in separating individual tree crowns of coniferous forest. The segmentation accuracy of mixed broadleaf and needle leaf trees obtained by Ke and Quackenbush (2008) was 61.3% which is quite similar to this study. Similarly, the accuracy which was obtained by Jing et al. (2012) in broadleaf forest is (65%) while in coniferous forest was 71%.

The over-segmented trees in this study was 1.39 and the under segmented was 0.57 (Table: 7). The over-segmentations happen when the area of reference objects is smaller than the result of automated segmentation. In contrast, under segmentation occurs when the real objects were smaller than the segmented result from automated segmentation. The over-segmentation was higher than under-segmentation because the heterogeneity of the objects in this study area was very high. Thus, the image was characterised noisy due to the high number of objects which these objects are forming their own watershed and regional minima (Jung & Scharcanski, 2002; Kim & Kim, 2003). A low pas smoothing filter (3 x 3) was applied to overcome this problem . However, the over-segmentation remained as an issue in this study because the study area has varying of tree crown size which requires different smoothing filter windows (Ke & Quackenbush, 2011).

There were four factors that effected to the result os segmentation. First, there was many several of local variance in the study area. It indicates by the peaks on ROC-LV graph (Figure 19). Mostly, the complex image shows such challenging graphs and complicating the interpretation of graphs (Drăguţ et al., 2010). The ROC-LV graphs (Figure 19) visualised the local variance in the study area which was relatively high. The study area has large local variety due to various crown texture, color, gaps and shadows. Figure 33 shows the variation condition in the study area. These noisy attributes led to produce low accuracy of segmentation (Ke et al., 2010). This multi-resolution can cause such a low accuracy of multi-resolution segmentation. Second, this algorithm is a user-dependent approach and quite relatively complex. The success of segmentation depends on the scale parameter, shape and compactness that were applied, thus the such segmentation result is common (Witharana & Civco, 2014). Third, the intermingled tree also contributes to such segmentation. The difficulty was that because the algorithm could not delineate a reasonable segment. Another possible reason was the distortion of the image. Therefore, the software could not perform reasonably to segment the objects because of disturbed visualisation on such images (Figure 32).

Figure 33: The condition in a part of study area

Figure 32: Image distortion

## 5.5. Model Development

Multiplicative log transformed regressions were established to develop the models to estimate aboveground biomass. Further discussions are given in the following sub-sections.

### 5.5.1. Relationship among variables

The relationship among variables were tested to analyse how strong the correlation between each variable and another. The linear relationship between DBH and height field measured was tested. The coefficient of determination and root mean square was 0.31 and 17.48 respectively, while the $R^2$ of DBH against height derived from point clouds was slightly higher (0.34) with RMSE 17.01. This result was lower than the result obtained by Khatry-Chhetri & Fowler (2006) in logged temperate broadleaf forest that was ranging from 0.41 to 0.52. The area of this study has a complex forest structure (terrain and vegetation). For instance: various levels of elevation, aspect, slope and species of trees and the competition between trees. These complexities made the tree height-DBH relationship and predictions become more complicated and did not provides reasonable accuracy (Fang & Bailey, 1998; Temesgen et al., 2013).

The linear relationship between DBH – automated CPA and DBH – crown diameter were also evaluated. The coefficient of determination values of the two tests were 0.02 for DBH – CPA and 0.12 for DBH – CPA. Theoretically, DBH and CPA should have a reasonable linear relation if there is less competition from neighbouring trees (Foli et al., 2003). The low values of $R^2$ of both tests in this study have indicated that there are high competition between neighbouring trees to access nutrient, growing space and light. The light competition happens when the crown of an individual tree touches its neighbours and forms the overlapped canopy (Shimano, 1997). This condition is similar to the study area (Figure 34 and Figure 35 show the overlapped canopies of such trees and the ground condition of these trees (as observed in the field).

The strength of relationships between DBH – AGB, CPA – AGB and CHM – AGB were evaluated using correlation analysis. The correlation value between DBH and AGB was the strongest relationship (0.96). It was as expected that DBH as one of strong predictor to above ground biomass measurement (Chave et al., 2005; Rutishauser et al., 2013). This is also because the calculation of AGB using allometric equation is strongly dependent on DBH. For variables which are extracted from 3D image point clouds, the correlation value between height derived from point cloud and above ground biomass was 0.66. This result was lower than the one obtained by Karna (2012) in the sub-tropical forest of Nepal which was ranging from 0.70 to 0.86. Karna (2012) used the allometric equation developed by Sharma and Pukkala (1990) to estimate field above ground biomass, and the choice of allometric equation is one possible reason in dissimilarities between the obtained the results. The result showed that the correlation of CPA and AGB has the lowest value due to the low accuracy of segmentation.

Figure 35: Overlapping trees on the study area

Figure 34: Ground condition on the field

### 5.5.2. Multiple regression between ln aboveground biomass, ln CPA and ln CHM

The log transformed multi-regression of aboveground biomass as dependent variable and log transformation of CPA and CHM as independent variables was established to develop a model of biomass estimation. The variables were transformed into natural logarithmic to correct the skeweness of data which do not fit with the requirements for parametric statistical tests (Sprugel, 1983). Several studies also established log transformation models to reduce bias in estimating biomass of tree (Chave et al., 2005; Feldpausch et al., 2012). Hence, the generic allometric equation by Chave et al. (2005) was applied to estimate above ground biomass using DBH and height from field measurement.

The coefficient of determination between CPA, CHM and biomass in log transformation was 0.57. This result is relatively low compared to the result obtained by Wangda (2012). Wangda (2012) established a log transformed allometric equation between CPA derived from rapid eye satellite image and CHM derived from LiDAR in the community forest of sub-tropical region in Nepal. The $R^2$ values were 0.74 for *Shorea robusta* and 0.76 for mixed species. The reason of obtaining lower $R^2$ in this study because the accuracy of automated CPA was low due to the complexity of forest characteristic in the study area. Nevertheless, there has been no study conducted in tropical rain forest to estimate aboveground biomass using automated segmented CPA and CHM from 3D aerial point clouds.

The $R^2$ value of data validation was 0.5996, which means the estimated above ground biomass can 59.96% be explained by predicted above ground biomass.

### 5.5.3. An alternative model (multiple regression between ln aboveground biomass, ln DBH measure in the field and ln CHM)

The alternative model was also evaluated that consider aboveground biomass as dependent variable and field measured diameter at breast height (DBH) and canopy height model (CHM) derived from 3D point clouds. It should be mentioned here that all variables are log transformed variables. The alternative model shows that the relationship between its variables was higher than the first model. The $R^2$ of alternative model which is using field measured DBH instead of segmented CPA was 0.9745. The reason of this issue, that there is an indication that the automated CPA was not a strong predictor for biomass estimation. Thus, segmented CPA was not related to the biomass estimation.

Several studies also used allometric models that use DBH and height as predictor to estimate biomass (Chave et al., 2005; Rutishauser et al., 2013). This model, however, was developed at plots level to estimate aboveground biomass and then the aboveground biomass of whole area can be generated.

The alternative model application is suggested at the plots level as proposed by several studies which used DBH and height as predictor variables (Feldpausch et al., 2012; Okuda et al., 2004). The use of tree height as predictive variable for biomass measurement improved the quality of the model (Chave et al., 2005). However, this variable usually is not available for censused trees. Since, the accuracy of CHM derived from point clouds is promising to estimate height of tree in the tropical forest. Thus, it can replace the field measurement of tree height.

Thus, the model that involves DBH and CHM from point clouds applied as alternative model for biomass estimation. The reason behind this is; because there are many uncertainties contributes to the accuracy of field height measurement . The study area has various slopes that lead to generate various land relief of the forest. This condition generates the issue of measured distance and tree-top position. The density of forest also contributes to get high accuracy of tree-top. The study area has high level of canopy closure, wide crowns and various tree heights, thus with these issue in mind it was difficult to recognise peak of canopy precisely (Larjavaara & Muller-Landau, 2013). Okuda et al (2004) demonstrated the biomass can be estimated using height derived from 3D photogrammetry. In addition, the aboveground biomass in the lowland Dipterocarp forest is highly correlated to height of tree .

### 5.6. Aboveground biomass/carbon stock estimation

The multi regression model that involved in log transformed CPA and log transformed CHM was used to estimate aboveground biomass. The estimated biomass in the study area was 146,810.04 Mg with an average of 190.51 Mg per ha. The above ground biomass was converted using the value of carbon fraction (IPCC, 2007)' Thus the carbon stock in the study area was estimated around 69,000 MgC and an average of 89.54 MgC per ha. Using the integration of ALOS PALSAR and field data in Borneo, Morel et al. (2011) obtained aboveground biomass in unlogged forest around 356Mg $ha^{-1}$ which is higher than the result of this study. It is this important to note that the study of Morel et al. (2011) is for primary (un-logged) forest while our study is in already logged-over forest. However, the result of this study is comparable to the logged tropical forest biomass in the Borneo forest that range between 150 Mg $ha^{-1}$ to 300 Mg $ha^{-1}$ (Berry et al., 2010; Kronseder et al., 2012). The reason for the dissimilar in obtaining biomass estimation is probably caused by the condition of study area and the choice of allometric equation.

### 5.7. Uncertaintes and source of errors for biomass/carbon stock mapping

Errors and uncertainties can be generated from collection, processing and analysis of data which are consequently accumulated and propagated through to the results (Wang et al., 2005). In the following sections we will discuss some of the sources of error.

#### 5.7.1. GPS

The navigation system used for data collection in the field was not adequate to locate the tree position that lead to misplacing the tree location on the image. The condition under dense canopy in a tropical rain forest considerably delays the GPS satellite signal acquisition that can noticeably be a source of error which reduce the accuracy and efficiency (Frank & Wing, 2013). If GPS with high accuracy of positioning level such as differential GPS could be implemented, the location of trees can be improved.

#### 5.7.2. Field tree estimation

Tree height is an essential variable for estimating aboveground biomass. However with such condition in the field, it was difficult to measure tree height very accurately. The height field measured process tends to overestimate the height of trees due to inaccurate tree-top recognition (Figure 36). A Haga altimeter was carried out to measure tree height in the field. The Haga altimeter has a lower accuracy than laser hypso-meter which regularly calibrated (Husch et al., 2003). Meanwhile, the accuracy of the laser instrument is overestimated ranging from +0.18 to ± 0.14 m (Clark et al., 2004). There were several possible uncertainties that contribute to the accuracy of field height measurement. These uncertainties are: the improper distance between viewing point and tree top position, tree top was blocking with other tree crowns, ground slope, creating problem for distance measurements and thus introducing Haga altimeter operator error (Hunter et al., 2013).

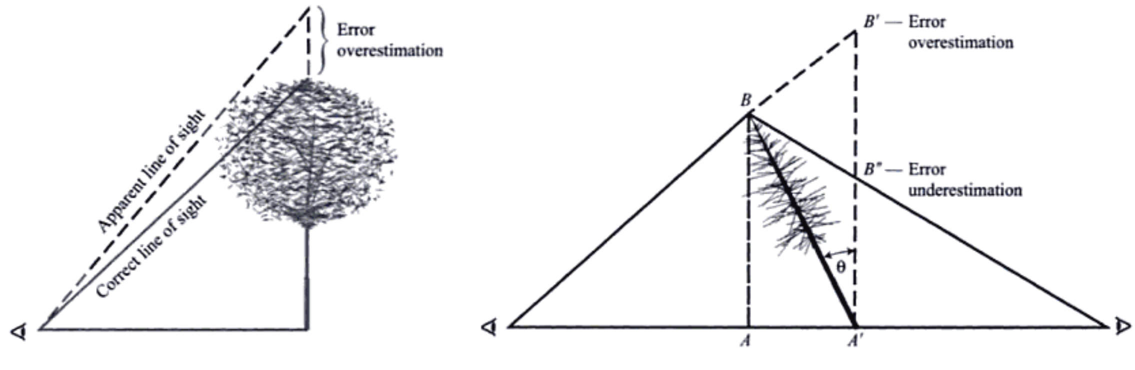


(a) Correctly identify top of tree (b) Estimate error of leaning trees

Figure 36: Errors in tree height measurement (Husch et al., 2003)

#### 5.7.3. Processing and analysis

**Canopy height model (CHM)**

A digital terrain model derived from 3D aerial point cloud was an issue influencing the accuracy of canopy height model. DTM accuracy usually depends on the condition of terrain slope, vegetation cover and the type of filtering algorithm that used in terrain model generation (Sithole & Vosselman, 2004). The DTM produced from 3D aerial point cloud was not highly accurate compared to DTM from LiDAR point clouds. The lack of accuracy on DTM by aerial point cloud influences the accuracy of its canopy height model.

**Image segmentation**

Image segmentation was a crucial step in this study. Theoretically, the scale parameter, shape and compactness on the algorithm influence the segmentation result (Benz et al., 2004). However, the segmentation accuracy showed that the error exists on the segmented result. The error occurred due to the complexities of the forest characteristics.

**Allometric equation**

The generic allometric equation by Chave et al. (2005) was used as suitable equation in this study because it has the lowest bias compared to local allometric equation by Basuki et al. (2009). However, the generic allometric also has an error to the actual aboveground biomass in certain forest (Rutishauser et al., 2013). The main source of uncertainty is the coefficient of *a* and *b* in allometric equation which is not calibrated for specific site (Ketterings et al., 2001).

### 5.8. Limitation of the research

1. GPS error in the field could not be avoided due to the forest condition in the study area (dense canopy, steep slope and various trees characteristic, for instance: crown size, height and species).
2. The ESP tool helped to determine the proper scale parameter through the ROC-LV graphs. However, trial and error scale parameter was carried out in multi-resolution segmentation. It almost never finds the perfect scale for a perfect segmentation in the object-based image analysis.

# 6. CONCLUSIONS AND RECOMMENDATIONS

## 6.1. Conclusion

In this study the combination of computer vision and object based image segmentation using point clouds derived from 3D aerial images to model above ground biomass in the tropical rain forest as a case study in Kelay concession, East Kalimantan, Indonesia has been evaluated. This research is one of the first studies of using computer vision technologies and automated object based segmentation in tropical rain forest. Nevertheless, the use of aerial images is promising to estimate and map above ground biomass of tropical rain forest. The following conclusions were reached based on the research questions:

***How accurately can height and CPA of individual tree of tropical rain forest be estimated from the point clouds extracted from 3D airborne imagesaerial photographs?***

The result obtained concluded that height derived from 3D aerial point clouds can explain 77.39% of height derived from field measured. The paired t test indicated that there is no difference between means of two heights at confident level 95%.

***What is the relationship between among diameter, CPA, height derived from 3D point clouds of optical 3D airborne images and aboveground biomass in the study area?***

Pearson's correlation analysis was conducted to test the correlation among variables which indicated that there is a strong relationship between field measured diameter and above ground biomass ($r>0.70$). The result also showed that the correlation between height derived from 3D aerial point cloud and aboveground biomass was higher than the correlation between automated segmentation of crown projection area and aboveground biomass.

***How can point clouds extracted from aerial-photos3D optical airborne images be used to improve the estimation of above ground biomass / carbon stock of tropical rain forest?***

The point clouds can improve the estimation of above ground biomass through its capability to estimate canopy height model. In the variables that were extracted from the point clouds of 3D images, the result showed that canopy height model was the more accurate predictor compared to segmented crown projection area. The correlation between canopy height model and above ground biomass was 0.66 which was higher than the correlation between CPA and carbon (0.21).

***How well can do model be developed by a point cloud extracted from 3D optical airborne images aerial photographs to estimate above ground biomass / carbon stock of the study area?***

The model was developed using log transformed multiplicative regression, which used lnCPA and lnCHM as independent variables and lnAGB as dependent variable. Thus the value of $R^2$ was 0.57. Model validation showed that the model was able to explain around 56.96% of carbon estimation variation. Although the result was relatively lower compare to other results, nevertheless there has been no study conducted for estimation above ground biomass using automated CPA and 3D point clouds derived height in the tropical rain forest. However, the alternative model which used lnDBH and lnCHM as independent variables and lnABG as dependent variable showed a stronger relationship ($R^2$ was 0.97 ) compared to the first model.

***How much above ground biomass / carbon stock are stored in the tropical rain forest of study area?***

Above ground biomass in the study area was estimated around 190.51 $MgHa^{-1}$ or 89.54 $MgCHa^{-1}$ of carbon stock.

## 6.2. Recommendation

This study in general demonstrated the usefulness of aerial image as low cost remote sensing method combined with computer vision method for extracting essential information from 3D images. Then, using those vital information the above ground biomass can be established. However, the result of automated segmentation was not satisfactory due to the forest characteristics in the study area. Nevertheless, the techniques that were used in this study are expected to contribute to a successful implementation of carbon valuation under REDD+ mechanism.

Height derived from 3D aerial point clouds showed very promising results. However, by combining a digital surface model derived from aerial point clouds with other high resolution digital terrain model such as LiDAR improve the accuracy of canopy height model.

The field validation should be improved using high accurate GPS such as differential GPS, so that the position error of location points can be minimised.

# LIST OF REFERENCES

Agisoft. (2012). Agisoft PhotoScan Professional edition. Retrieved 18 August 2013, 2013, from http://agisoft.ru/products/photoscan/professional/

Andersson, K., Evans, T. P., & Richards, K. R. (2009). National forest carbon inventories: policy needs and assessment capacity. *Climatic Change, 93*(1-2), 69-101. doi: 10.1007/s10584-008-9526-6

Baatz, M., & Schäpe, A. (2000). Multiresolution segmentation: an optimization approach for high quality multi-scale image segmentation. *Angewandte geographische informationsverarbeitung, 12*(12), 12-23.

Baillard, C. (2003). Production of DSM/DTM in urban areas: Role and influence of 3-D vectors. *ISPRS Archives, 34*(Part 3), W8.

Barr, C., Resosudarmo, I. A. P., Dermawan, A., McCarthy, J. F., Moeliono, M., Setiono, B., & eds. (2006). *Decentralization of forest administration in Indonesia: implications for forest sustainability, economic development and community livelihoods*. Bogor, Indonesia: Center for International Forestry Research (CIFOR).

Bársony, C. A., Ciais, P., Viovy, N., & Vuichard, N. (2011). REDD Mitigation. *Procedia Environmental Sciences, 6*(0), 50-59. doi: http://dx.doi.org/10.1016/j.proenv.2011.05.006

Basuki, T. M., van Laake, P. E., Skidmore, A. K., & Hussin, Y. A. (2009). Allometric equations for estimating the above-ground biomass in tropical lowland Dipterocarp forests. *Forest Ecology and Management, 257*(8), 1684-1694. doi: http://dx.doi.org/10.1016/j.foreco.2009.01.027

Benz, U. C., Hofmann, P., Willhauck, G., Lingenfelder, I., & Heynen, M. (2004). Multi-resolution, object-oriented fuzzy analysis of remote sensing data for GIS-ready information. *ISPRS Journal of Photogrammetry and Remote Sensing, 58*(3–4), 239-258. doi: http://dx.doi.org/10.1016/j.isprsjprs.2003.10.002

Berry, N. J., Phillips, O. L., Lewis, S. L., Hill, J. K., Edwards, D. P., Tawatao, N. B., . . . Hamer, K. C. (2010). The high value of logged tropical forests: Lessons from northern Borneo. *Biodiversity and Conservation, 19*(4), 985-997.

Beucher, S. (1992). The watershed transformation applied to image segmentation. *SCANNING MICROSCOPY-SUPPLEMENT-*, 299-299.

Blaschke, T. (2010). Object based image analysis for remote sensing. *ISPRS Journal of Photogrammetry and Remote Sensing, 65*(1), 2-16. doi: http://dx.doi.org/10.1016/j.isprsjprs.2009.06.004

Bohlin, J., Wallerman, J., & Fransson, J. E. S. (2012). Forest variable estimation using photogrammetric matching of digital aerial images in combination with a high-resolution DEM. *Scandinavian Journal of Forest Research, 27*(7), 692-699. doi: 10.1080/02827581.2012.686625

Braatz, S. (2008). Working with Countries to Reduce Deforestation and Forest Degradation: Taking Climate Change Action through Sustainable Forest Management (F. Department, Trans.). Rome: FAO.

Brown, S. (1997). *Estimating biomass and biomass change of tropical forests: a primer* (Vol. 134). Rome: FAO.

Brown, S., Pearson, T., Slaymaker, D., Ambagis, S., Moore, N., Novelo, D., & Sabido, W. (2005). Creating a Virtual Tropical Forest from Three-Dimensional Aerial Imagery to Estimate Carbon Stocks. *Ecological Applications, 15*(3), 1083-1095. doi: 10.2307/4543417

Butler, R. (2012). Tropical Rainforests Of The World. Retrieved August 3, 2013, from http://rainforests.mongabay.com/0101.htm

Chave, J., Andalo, C., Brown, S., Cairns, M. A., Chambers, J. Q., Eamus, D., . . . Yamakura, T. (2005). Tree allometry and improved estimation of carbon stocks and balance in tropical forests. *Oecologia, 145*(1), 87-99. doi: 10.1007/s00442-005-0100-x

Chen, Q., Vaglio Laurin, G., Battles, J. J., & Saah, D. (2012). Integration of airborne lidar and vegetation types derived from aerial photography for mapping aboveground live biomass. *Remote Sensing of Environment, 121*(0), 108-117. doi: http://dx.doi.org/10.1016/j.rse.2012.01.021

Childs, C. (2004). Interpolating Surface in ArcGIS Spatial Analyst. http://www.esri.com/news/arcuser/0704/files/interpolating.pdf

CIFOR. (2009). Simply REDD: CIFOR's guide to forests, climate change and REDD. Retrieved 2 June, 2013, from http://www.cifor.org/publications/pdf_files/media/MediaGuide_REDD.pdf

Clark, M. L., Clark, D. B., & Roberts, D. A. (2004). Small-footprint lidar estimation of sub-canopy elevation and tree height in a tropical rain forest landscape. *Remote Sensing of Environment, 91*(1), 68-89. doi: http://dx.doi.org/10.1016/j.rse.2004.02.008

Clinton, N., Holt, A., Scarborough, J., Yan, L., & Gong, P. (2010). Accuracy assessment measures for object-based image segmentation goodness. *Photogrammetric Engineering and Remote Sensing, 76*(3), 289-299.

Cramer, M., Stallmann, D., & Haala, N. (2000). Direct georeferencing using GPS/inertial exterior orientations for photogrammetric applications. *International Archives of Photogrammetry and Remote Sensing, 33*(B3/1; PART 3), 198-205.

Dandois, J. P., & Ellis, E. C. (2010). Remote Sensing of Vegetation Structure Using Computer Vision. *Remote Sensing, 2*(4), 1157-1176.

Dandois, J. P., & Ellis, E. C. (2013). High spatial resolution three-dimensional mapping of vegetation spectral dynamics using computer vision. *Remote Sensing of Environment, 136*(0), 259-276. doi: http://dx.doi.org/10.1016/j.rse.2013.04.005

Derivaux, S., Forestier, G., Wemmert, C., & Lefèvre, S. (2010). Supervised image segmentation using watershed transform, fuzzy classification and evolutionary computation. *Pattern Recognition Letters, 31*(15), 2364-2374. doi: http://dx.doi.org/10.1016/j.patrec.2010.07.007

DOF. (2004). Community Forest Inventory Guidelines *Community Forest Division*. Kathmandu, Nepal: Department of Forests

Drăguţ, L., Tiede, D., & Levick, S. R. (2010). ESP: a tool to estimate scale parameter for multiresolution image segmentation of remotely sensed data. *International Journal of Geographical Information Science, 24*(6), 859-871. doi: 10.1080/13658810903174803

Drake, J. B., Knox, R. G., Dubayah, R. O., Clark, D. B., Condit, R., Blair, J. B., & Hofton, M. (2003). Above-ground biomass estimation in closed canopy Neotropical forests using lidar remote sensing: factors affecting the generality of relationships. *Global Ecology and Biogeography, 12*(2), 147-159. doi: DOI 10.1046/j.1466-822X.2003.00010.x

Dubayah, R. O., & Drake, J. B. (2000). Lidar remote sensing for forestry. *Journal of Forestry, 98*(6), 44-46.

Elevitch, C. R., & Manner, H. I. (2006). Artocarpus heterophyllus (jackfruit). *Species Profiles for Pacific Island Agroforestry, ver.I.IV*.

Fabris, M., & Pesci, A. (2005). *Automated DEM extraction in digital aerial photogrammetry: precisions and validation for mass movement monitoring* (Vol. 48).

Fang, Z., & Bailey, R. L. (1998). Height–diameter models for tropical forests on Hainan Island in southern China. *Forest Ecology and Management, 110*(1–3), 315-327. doi: http://dx.doi.org/10.1016/S0378-1127(98)00297-7

FAO. (2010). Global Forest Resources Assessment 2010 *FAO Forestry paper*. Rome: Food and Agriculture Organization of The United Nation.

Feldpausch, T., Lloyd, J., Lewis, S., Brienen, R., Gloor, E., Monteagudo Mendoza, A., . . . Affum-Baffoe, K. (2012). Tree height integrated into pan-tropical forest biomass estimates. *Biogeosciences Discussions, 9*(3), 2567-2622.

Foli, E. G., Alder, D., Miller, H. G., & Swaine, M. D. (2003). Modelling growing space requirements for some tropical forest tree species. *Forest Ecology and Management, 173*(1–3), 79-88. doi: http://dx.doi.org/10.1016/S0378-1127(01)00815-5

Frank, J., & Wing, M. G. (2013). Differential GPS effectiveness in measuring area and perimeter in forested settings. *Measurement Science and Technology, 24*(10), 105801.

Gao, Y., Mas, J. F., Kerle, N., & Navarrete Pacheco, J. A. (2011). Optimal region growing segmentation and its effect on classification accuracy. *International Journal of Remote Sensing, 32*(13), 3747-3763. doi: 10.1080/01431161003777189

Gibbs, H. K., Brown, S., Niles, J. O., & Foley, J. A. (Writers). (2007). Monitoring and estimating tropical forest carbon stocks: making REDD a reality. In IOPscience (Producer).

Goetz, S., & Dubayah, R. (2011). Advances in remote sensing technology and implications for measuring and monitoring forest carbon stocks and change. *Carbon Management, 2*(3), 231-244.

Gonzalez, P., Asner, G. P., Battles, J. J., Lefsky, M. A., Waring, K. M., & Palace, M. (2010). Forest carbon densities and uncertainties from Lidar, QuickBird, and field measurements in California. *Remote Sensing of Environment, 114*(7), 1561-1575. doi: http://dx.doi.org/10.1016/j.rse.2010.02.011

He, Z., Zhao, W., Liu, H., & Zhang, Z. (2010). Successional process of Picea crassifolia forest after logging disturbance in semiarid mountains: A case study in the Qilian Mountains, northwestern China. *Forest Ecology and Management, 260*(3), 396-402. doi: http://dx.doi.org/10.1016/j.foreco.2010.04.034

Hudak, A. T., Crookston, N. L., Evans, J. S., Falkowski, M. J., Smith, A. M., Gessler, P. E., & Morgan, P. (2006). Regression modeling and mapping of coniferous forest basal area and tree density from discrete-return lidar and multispectral satellite data. *Canadian Journal of Remote Sensing, 32*(2), 126-138.

Hunter, M., Keller, M., Vitoria, D., & Morton, D. (2013). Tree height and tropical forest biomass estimation. *Biogeosciences Discussions, 10*(6), 10491-10529.

Husch, B., Beers, T. W., & Kershaw, J. A. (2003). *Forest mensuration* (Fourth edition ed.). Hoboken: Wiley & Sons.

Pedoman Pelaksanaan Sistem Silvikultur Tebang Pilih Tanam Indonesia (TPTI), P.9/VI-BPHA/2009 C.F.R. (2009).

IPCC. (2006). *Guidelines for National Greenhouse Gas Inventories* (Vol. 4). Hayama, Japan: Institute for Global Environmental Strategies (IGES).

IPCC. (2007). Climate Change 2007: The Physical Science Basis. Contribution of Working Group I to the Fourth Assessment Report of the Intergovernmental Panel on Climate Change (pp. 996). Cambridge, United Kingdom and New York, NY, USA.

ITTO. (2000). Auditing Of Sustainable Forest Management: A practical guide for developing local auditing systems based on ITTO's Criteria and Indicators. *Working paper 4.*

Järnstedt, J., Pekkarinen, A., Tuominen, S., Ginzler, C., Holopainen, M., & Viitala, R. (2012). Forest variable estimation using a high-resolution digital surface model. *ISPRS Journal of Photogrammetry and Remote Sensing, 74*(0), 78-84. doi: http://dx.doi.org/10.1016/j.isprsjprs.2012.08.006

Jing, L., Hu, B., Noland, T., & Li, J. (2012). An individual tree crown delineation method based on multi-scale segmentation of imagery. *ISPRS Journal of Photogrammetry and Remote Sensing, 70*(0), 88-98. doi: http://dx.doi.org/10.1016/j.isprsjprs.2012.04.003

Jung, C. R., & Scharcanski, J. (2002). *Robust watershed segmentation using the wavelet transform.* Paper presented at the Computer Graphics and Image Processing, 2002. Proceedings. XV Brazilian Symposium on.

Karna, Y. K. (2012). *Mapping above ground carbon using worldview satellite image and LIDAR data in relationship with tree diversity of forests.* University of Twente Faculty of Geo-Information and Earth Observation (ITC), Enschede. Retrieved from http://www.itc.nl/library/papers_2012/msc/nrm/karna.pdf

Ke, Y., & Quackenbush, L. J. (2008). *Comparison of individual tree crown detection and delineation methods.* Paper presented at the Proceedings of 2008 ASPRS Annual Conference, American Society of Photogrammetry and Remote Sensing.

Ke, Y., & Quackenbush, L. J. (2011). A review of methods for automatic individual tree-crown detection and delineation from passive remote sensing. *International Journal of Remote Sensing, 32*(17), 4725-4747. doi: 10.1080/01431161.2010.494184

Ke, Y., Quackenbush, L. J., & Im, J. (2010). Synergistic use of QuickBird multispectral imagery and LIDAR data for object-based forest species classification. *Remote Sensing of Environment, 114*(6), 1141-1154.

Ketterings, Q. M., Coe, R., van Noordwijk, M., Ambagau, Y., & Palm, C. A. (2001). Reducing uncertainty in the use of allometric biomass equations for predicting above-ground tree biomass in mixed secondary forests. *Forest Ecology and Management, 146*(1), 199-209.

Khatry-Chhetri, D. B., & Fowler, G. W. (1996). Prediction models for estimating total heights of trees from diameter at breast height measurements in Nepal's lower temperate broad-leaved forests. *Forest Ecology and Management, 84*(1–3), 177-186. doi: http://dx.doi.org/10.1016/0378-1127(96)03726-7

Kim, J. B., & Kim, H. J. (2003). Multiresolution-based watersheds for efficient image segmentation. *Pattern Recognition Letters, 24*(1), 473-488.

Kim, M., Madden, M., & Warner, T. (2008). Estimation of optimal image object size for the segmentation of forest stands with multispectral IKONOS imagery. In T. Blaschke, S. Lang & G. Hay (Eds.), *Object-Based Image Analysis* (pp. 291-307): Springer Berlin Heidelberg.

Kim, M., Warner, T. A., Madden, M., & Atkinson, D. S. (2011). Multi-scale GEOBIA with very high spatial resolution digital aerial imagery: scale, texture and image objects. *International Journal of Remote Sensing, 32*(10), 2825-2850. doi: 10.1080/01431161003745608

Koch, B. (2010). Status and future of laser scanning, synthetic aperture radar and hyperspectral remote sensing data for forest biomass assessment. *ISPRS Journal of Photogrammetry and Remote Sensing, 65*(6), 581-590. doi: http://dx.doi.org/10.1016/j.isprsjprs.2010.09.001

Köhl, M., Baldauf, T., Plugge, D., & Krug, J. (2009). Reduced emissions from deforestation and forest degradation (REDD): a climate change mitigation strategy on a critical track. *Carbon Balance and Management, 4*(10), 1-10.

Korpela, I. (2004). Individual Tree Measurements by Means of Digital Aerial Photogrammetry. *Silva Fennica*.

Kronseder, K., Ballhorn, U., Böhm, V., & Siegert, F. (2012). Above ground biomass estimation across forest types at different degradation levels in Central Kalimantan using LiDAR data. *International Journal of Applied Earth Observation and Geoinformation, 18*(0), 37-48. doi: http://dx.doi.org/10.1016/j.jag.2012.01.010

Kwak, D.-A., Lee, W.-K., Lee, J.-H., Biging, G., & Gong, P. (2007). Detection of individual trees and estimation of tree height using LiDAR data. *Journal of Forest Research, 12*(6), 425-434. doi: 10.1007/s10310-007-0041-9

Lackmann, S. (2011). Good Practice in Designing a Forest Inventory Quito, Ecuador: Coalition for Rainforest Nations

Lamonaca, A., Corona, P., & Barbati, A. (2008). Exploring forest structural complexity by multi-scale segmentation of VHR imagery. *Remote Sensing of Environment, 112*(6), 2839-2849.

Larjavaara, M., & Muller-Landau, H. C. (2013). Measuring tree height: a quantitative comparison of two common field methods in a moist tropical forest. *Methods in Ecology and Evolution, 4*(9), 793-801. doi: 10.1111/2041-210X.12071

Leberl, F., Irschara, A., Pock, T., Meixner, P., Gruber, M., Scholz, S., & Wiechert, A. (2010). Point Clouds: Lidar versus 3D Vision. *Published in Photogrammetric Engineering and Remote Sensing, 76*(10), 1123.

Lillesand, T. M., Kiefer, R. W., & Chipman, J. W. (2008). *Remote sensing and image interpretation* (Sixth edition ed.). New York: Wiley & Sons.

Lisein, J., Pierrot-Deseilligny, M., Bonnet, S., & Lejeune, P. (2013). A Photogrammetric Workflow for the Creation of a Forest Canopy Height Model from Small Unmanned Aerial System Imagery. *Forests, 4*(4), 922-944.

Lowe, D. G. (2004). Distinctive image features from scale-invariant keypoints. *International journal of computer vision, 60*(2), 91-110.

Lucas, R., Bunting, P., Paterson, M., & Chisholm, L. (2008). Classification of Australian forest communities using aerial photography, CASI and HyMap data. *Remote Sensing of Environment, 112*(5), 2088-2103. doi: http://dx.doi.org/10.1016/j.rse.2007.10.011

Lucieer, A., Turner, D., King, D. H., & Robinson, S. A. (2014). Using an Unmanned Aerial Vehicle (UAV) to capture micro-topography of Antarctic moss beds. *International Journal of Applied Earth Observation and Geoinformation, 27, Part A*(0), 53-62. doi: http://dx.doi.org/10.1016/j.jag.2013.05.011

Mandallaz, D. (2008). *Sampling techniques for forest inventories*. Boca Raton: Chapman & Hall.

Marpu, P. R., Neubert, M., Herold, H., & Niemeyer, I. (2010). Enhanced evaluation of image segmentation results. *Journal of Spatial Science, 55*(1), 55-68. doi: 10.1080/14498596.2010.487850

Mbaabu, P. R. (2012). *AGB carbon mapping using airborne LIDAR data and geo-eye satellite images in tropical forests of Chitwan, Nepal : a comparison of community and government managed forests*. University of Twente Faculty of Geo-Information and Earth Observation (ITC), Enschede. Retrieved from http://www.itc.nl/library/papers_2012/msc/nrm/mbaabu.pdf

Meia, C., & Durrieub, S. (2004). Tree Crown Delineation From Digital Elevation Models And High Resolution Imagery. *International Society for Photogrammetry and Remote Sensing*.

MoF. (2008). Consolidation Report : Reducing Emissions from Deforestation and Forest Degradation in Indonesia. Jakarta: Ministry of Forestry of the Republic of Indonesia.

Möller, M., Lymburner, L., & Volk, M. (2007). The comparison index: A tool for assessing the accuracy of image segmentation. *International Journal of Applied Earth Observation and Geoinformation, 9*(3), 311-321. doi: http://dx.doi.org/10.1016/j.jag.2006.10.002

Mora, B., Wulder, M. A., & White, J. C. (2010). Segment-constrained regression tree estimation of forest stand height from very high spatial resolution panchromatic imagery over a boreal environment. *Remote Sensing of Environment, 114*(11), 2474-2484. doi: http://dx.doi.org/10.1016/j.rse.2010.05.022

Morel, A. C., Saatchi, S. S., Malhi, Y., Berry, N. J., Banin, L., Burslem, D., . . . Ong, R. C. (2011). Estimating aboveground biomass in forest and oil palm plantation in Sabah, Malaysian Borneo using ALOS PALSAR data. *Forest Ecology and Management, 262*(9), 1786-1798. doi: DOI 10.1016/j.foreco.2011.07.008

Muhdi. (2005). Pemanenan Kayu Dalam Sistem Tebang Pilih Tanam Indonesia (TPTI). Medan, Indonesia: Universitas Sumatera Utara.

Niethammer, U., James, M. R., Rothmund, S., Travelletti, J., & Joswig, M. (2012). UAV-based remote sensing of the Super-Sauze landslide: Evaluation and results. *Engineering Geology, 128*, 2-11.

Nurminen, K., Karjalainen, M., Yu, X., Hyyppä, J., & Honkavaara, E. (2013). Performance of dense digital surface models based on image matching in the estimation of plot-level forest variables. *ISPRS Journal of Photogrammetry and Remote Sensing, 83*(0), 104-115. doi: http://dx.doi.org/10.1016/j.isprsjprs.2013.06.005

Okuda, T., Suzuki, M., Adachi, N., Quah, E. S., Hussein, N. A., & Manokaran, N. (2003). Effect of selective logging on canopy and stand structure and tree species composition in a lowland dipterocarp forest in peninsular Malaysia. *Forest Ecology and Management, 175*(1–3), 297-320. doi: http://dx.doi.org/10.1016/S0378-1127(02)00137-8

Okuda, T., Suzuki, M., Numata, S., Yoshida, K., Nishimura, S., Adachi, N., . . . Hashim, M. (2004). Estimation of aboveground biomass in logged and primary lowland rainforests using 3-D photogrammetric analysis. *Forest Ecology and Management, 203*(1–3), 63-75. doi: http://dx.doi.org/10.1016/j.foreco.2004.07.056

Pearce, D. (2001). How Valuable Are The Tropical Forests? Demonstrating And Capturing Economic Value As A Means Of Addressing The Causes Of Deforestation. *Seminar paper for Conseil d'Analyse Économique*.

Popescu, S. C. (2007). Estimating biomass of individual pine trees using airborne lidar. *Biomass and Bioenergy, 31*(9), 646-655.

Pouliot, D. A., King, D. J., Bell, F. W., & Pitt, D. G. (2002). Automated tree crown detection and delineation in high-resolution digital camera imagery of coniferous forest regeneration. *Remote Sensing of Environment, 82*(2–3), 322-334. doi: http://dx.doi.org/10.1016/S0034-4257(02)00050-0

Priyadi, H. (2007). *Towards Sustainable Forest Management by Implementation of Reduced-Impact Logging (RIL) Techniques in Indonesia with References in Kalimantan.* Paper presented at the Open Science Meetings.

PROSEA. (2013). *Wood Density Database*. Retrieved from: http://www.worldagroforestrycentre.org/sea/Products/AFDbases/wd/index.htm

Pulighe, G., & Fava, F. (2013). DEM extraction from archive aerial photos: accuracy assessment in areas of complex topography. *European Journal of Remote Sensing, 46*, 363-378. doi: 10.5721/EuJRS20134621

Qureshi, A., Pariva, Badola, R., & Hussain, S. A. (2012). A review of protocols used for assessment of carbon stock in forested landscapes. *Environmental Science & Policy, 16*(0), 81-89. doi: http://dx.doi.org/10.1016/j.envsci.2011.11.001

Rutishauser, E., Noor'an, F., Laumonier, Y., Halperin, J., Rufi'ie, Hergoualc'h, K., & Verchot, L. (2013). Generic allometric models including height best estimate forest biomass and carbon stocks in Indonesia. *Forest Ecology and Management, 307*(0), 219-225. doi: http://dx.doi.org/10.1016/j.foreco.2013.07.013

Saner, P., Loh, Y. Y., Ong, R. C., & Hector, A. (2012). Carbon Stocks and Fluxes in Tropical Lowland Dipterocarp Rainforests in Sabah, Malaysian Borneo. *PLoS ONE, 7*(1), e29642. doi: 10.1371/journal.pone.0029642

Schmidt, F. H., & Ferguson, J. H. A. (1951). *Rainfall Types Based on Wet and Dry Period Ratios for Indonesia with Western New Guinee*. Djakarta: Djawatan Meteorologi dan Geofisik.

Sharma, E. R., & Pukkala, T. (1990). *Volume Equations and Biomass Prediction of Forest Trees of Nepal*. Kathmandu, Nepal.

Shiba, M., & Itaya, A. (2005). using eCognition for improved forest management and monitoring systems in precision forestry

Shimano, K. (1997). Analysis of the relationship between DBH and crown projection area using a new model. *Journal of Forest Research, 2*(4), 237-242. doi: 10.1007/BF02348322

Shiver, B. D., & Borders, B. E. (1996). *Sampling techniques for forest resource inventory*: John Wiley and Sons.

Sithole, G., & Vosselman, G. (2004). Experimental comparison of filter algorithms for bare-Earth extraction from airborne laser scanning point clouds. *ISPRS Journal of Photogrammetry and Remote Sensing, 59*(1–2), 85-101. doi: http://dx.doi.org/10.1016/j.isprsjprs.2004.05.004

Slik, J. W. F., Verburg, R., & Keßler, P. A. (2002). Effects of fire and selective logging on the tree species composition of lowland dipterocarp forest in East Kalimantan, Indonesia. *Biodiversity & Conservation, 11*(1), 85-98. doi: 10.1023/A:1014036129075

Snavely, N., Seitz, S. M., & Szeliski, R. (2007). Modeling the world from internet photo collections. *Proc. IJCV*, 189-210.

Sprugel, D. (1983). Correcting for bias in log-transformed allometric equations. *Ecology, 64*(1), 209-210.

St-Onge, B., Vega, C., Fournier, R. A., & Hu, Y. (2008). Mapping canopy height using a combination of digital stereo-photogrammetry and lidar. *International Journal of Remote Sensing, 29*(11), 3343-3364. doi: 10.1080/01431160701469040

Straub, C., Tian, J., Seitz, R., & Reinartz, P. (2013). Assessment of Cartosat-1 and WorldView-2 stereo imagery in combination with a LiDAR-DTM for timber volume estimation in a highly structured forest in Germany. *Forestry, 86*(4), 463-473. doi: 10.1093/forestry/cpt017

Suárez, J. C., Ontiveros, C., Smith, S., & Snape, S. (2005). Use of airborne LiDAR and aerial photography in the estimation of individual tree heights in forestry. *Computers & Geosciences, 31*(2), 253-262. doi: http://dx.doi.org/10.1016/j.cageo.2004.09.015

Tao, W., Lei, Y., & Mooney, P. (2011). *Dense point cloud extraction from UAV captured images in forest area.* Paper presented at the Spatial Data Mining and Geographical Knowledge Services (ICSDM), 2011 IEEE International Conference on.

Temesgen, H., Zhang, C., & Zhao, X. (2013). Modelling tree height–diameter relationships in multi-species and multi-layered forests: A large observational study from Northeast China. *Forest Ecology and Management*.

Tian, J., & Chen, D. M. (2007). Optimization in multi-scale segmentation of high-resolution satellite images for artificial feature recognition. *International Journal of Remote Sensing, 28*(20), 4625-4644. doi: 10.1080/01431160701241746

Tiede, D., Lang, S., & Hoffmann, C. (2006). Supervised and forest type-specific multi-scale segmentation for a one-level-representation of single trees. *International Archives of Photogrammetry, Remote Sensing and Spatial Information Sciences, 36*, 4.

Tiwari, A. K., & Singh, J. S. (1984). Mapping forest biomass in India through aerial photographs and nondestructive field sampling. *Applied Geography, 4*(2), 151-165. doi: http://dx.doi.org/10.1016/0143-6228(84)90019-5

Trimble. (2011a). *eCognition Developer 8.7: User Guide*. Munchen, Germany: Trimble Germany GmbH.

Trimble. (2011b). *eCognition Developer 8.7: Reference Book*. Munchen, Germany: Trimble Germany GmbH.

Tsendbazar, N. E. (2011). *Object based image analysis of geo - eye VHR data to model above ground carbon stock in Himalayan mid - hill forests, Nepal.* University of Twente Faculty of Geo-Information and Earth Observation (ITC), Enschede. Retrieved from http://www.itc.nl/library/papers_2011/msc/nrm/tsendbazar.pdf

Turner, D., Lucieer, A., & Watson, C. (2012). An automated technique for generating georectified mosaics from ultra-high resolution unmanned aerial vehicle (UAV) imagery, based on structure from motion (SfM) point clouds. *Remote Sensing, 4*(5), 1392-1410.

Ullman, S. (1979). The interpretation of structure from motion. *Proceedings of the Royal Society of London. Series B. Biological Sciences, 203*(1153), 405-426.

UN-REDD. (2013). National Forest Monitoring Systems: Monitoring and Measurement, Reporting and Verification (M & MRV) in the context of REDD+ Activities. Châtelaine, Geneva, Switzerland: UN-REDD.

UNFCC. (2009). Methodological guidance for activities relating to reducing emissions from deforestation and forest degradation and the role of conservation, sustainable management of forests and enhancement of forest carbon stocks in developing countries. Bonn, Germany: United Nations Framework Convention on Climate Change.

Valérie, T., & Marie-Pierre, J. (2006). Tree species identification on large-scale aerial photographs in a tropical rain forest, French Guiana—application for management and conservation. *Forest Ecology and Management, 225*(1–3), 51-61. doi: http://dx.doi.org/10.1016/j.foreco.2005.12.046

Verhoeven, G. (2011). Taking computer vision aloft – archaeological three-dimensional reconstructions from aerial photographs with photoscan. *Archaeological Prospection, 18*(1), 67-73. doi: 10.1002/arp.399

Verhoeven, G., Doneus, M., Briese, C., & Vermeulen, F. (2012). Mapping by matching: a computer vision-based approach to fast and accurate georeferencing of archaeological aerial photographs. *Journal of Archaeological Science, 39*(7), 2060-2070. doi: http://dx.doi.org/10.1016/j.jas.2012.02.022

Walker, J. S., & Briggs, J. M. (2005). *An object-oriented classification of an arid urban forest with true-color aerial photography*.

Wang, G., Gertner, G. Z., Fang, S., & Anderson, A. (2005). A methodology for spatial uncertainty analysis of remote sensing and GIS products. *Photogrammetric Engineering and Remote Sensing, 71*(12), 1423.

Wang, L., Chen, E., Li, Z., Yao, W., & Li, S. (2013). *Object-based analysis for forest inventory.* Paper presented at the Eighth International Symposium on Multispectral Image Processing and Pattern Recognition.

Wang, L., Gong, P., & Biging, G. S. (2004). Individual tree-crown delineation and treetop detection in high-spatial-resolution aerial imagery. *Photogrammetric Engineering and Remote Sensing, 70*(3), 351-358.

Wangda, P. (2012). *Upscalling The Estimated Forest Carbon Stock from VHR Satellite Image and Airborne Lidar to Rapideye Satellite Image.* (Master), University of Twente, Enschede, The Netherlands.

Witharana, C., & Civco, D. L. (2014). Optimizing multi-resolution segmentation scale using empirical methods: Exploring the sensitivity of the supervised discrepancy measure Euclidean distance 2 (ED2). *ISPRS Journal of Photogrammetry and Remote Sensing, 87*(0), 108-121. doi: http://dx.doi.org/10.1016/j.isprsjprs.2013.11.006

Wohler, C. (2013). *3D computer vision: efficient methods and applications*: Springer.

Wolf, P. R., & Dewitt, B. A. (2000). *Elements of photogrammetry : with applications in GIS*. Boston etc.: McGraw-Hill.

Woodcock, C. E., & Strahler, A. H. (1987). The factor of scale in remote sensing. *Remote Sens. Environ., 21*(3), 311-332. doi: 10.1016/0034-4257(87)90015-0

World-Bank. (2013). *Indonesia* [Time series]. Retrieved from: http://data.worldbank.org/country/indonesia

Yang, B., Shi, W., & Li, Q. (2005). A dynamic method for generating multi-resolution TIN models. *Photogrammetric Engineering and Remote Sensing, 71*(8), 917.

Zhang, K., Chen, S.-C., Whitman, D., Shyu, M.-L., Yan, J., & Zhang, C. (2003). A Progressive Morphological Filter for Removing Nonground Measurements From Airborne LIDAR Data. *IEEE Transactions On Geoscience And Remote Sensing, 41*(4).

Zhang, Y. J. (1996). A survey on evaluation methods for image segmentation. *Pattern Recognition, 29*(8), 1335-1346. doi: http://dx.doi.org/10.1016/0031-3203(95)00169-7

Zhao, F., Guo, Q., & Kelly, M. (2012). Allometric equation choice impacts lidar-based forest biomass estimates: A case study from the Sierra National Forest, CA. *Agricultural and Forest Meteorology, 165*(0), 64-72. doi: http://dx.doi.org/10.1016/j.agrformet.2012.05.019

# APPENDICES

Appendix 1: Sample plots location

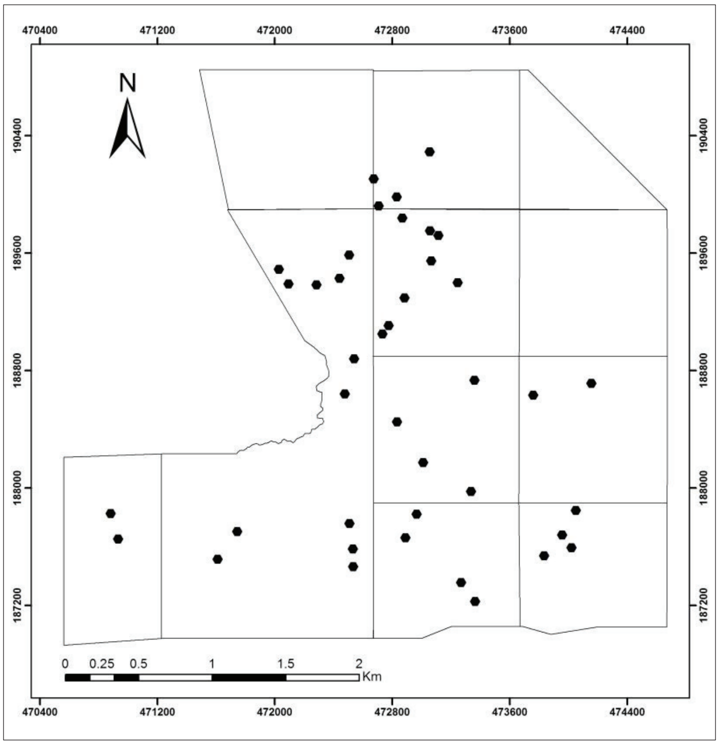


Appendix 2: Camera locations and image overlap

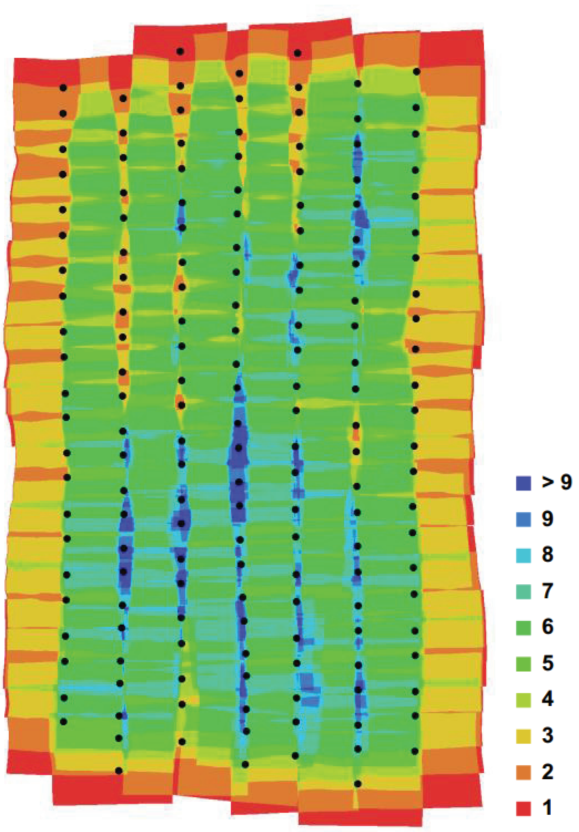

Appendix 3: Camera locations and error estimates

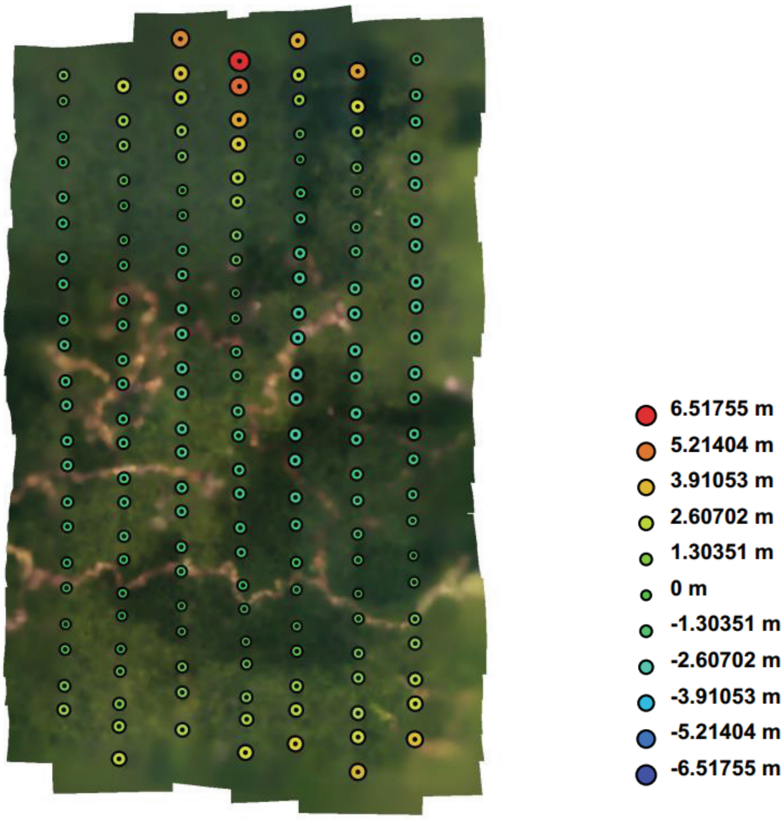


| Horizontal error (m) | Vertical error (m) | Total error (m) |
|---|---|---|
| 0.833899 | 1.832907 | 2.242364 |

Appendix 4: Normality test for model development variables

Skewness/Kurtosis tests for Normality

| Variable | Obs | Pr(Skewness) | Pr(Kurtosis) | joint adj chi2(2) | joint Prob>chi2 |
|---|---|---|---|---|---|
| CHM | 31 | 0.5013 | 0.6785 | 0.65 | 0.7221 |
| CPA | 31 | 0.0009 | 0.0045 | 14.53 | 0.0007 |

Appendix 5: Anova and regression results among variables

```
. regress DBH H

      Source |       SS       df       MS              Number of obs =      31
-------------+------------------------------           F(  1,    29) =   13.10
       Model |  4004.31499     1  4004.31499           Prob > F      =  0.0011
    Residual |  8865.03985    29  305.691029           R-squared     =  0.3112
-------------+------------------------------           Adj R-squared =  0.2874
       Total |  12869.3548    30  428.978495           Root MSE      =  17.484

------------------------------------------------------------------------------
         DBH |      Coef.   Std. Err.      t    P>|t|     [95% Conf. Interval]
-------------+----------------------------------------------------------------
           H |    1.14687   .3168775     3.62   0.001     .4987827    1.794957
       _cons |   5.501166   10.40059     0.53   0.601    -15.77042    26.77275
------------------------------------------------------------------------------
```

```
. regress DBH CPA

      Source |       SS       df       MS              Number of obs =      31
-------------+------------------------------           F(  1,    29) =    0.79
       Model |  343.114435     1  343.114435           Prob > F      =  0.3801
    Residual |  12526.2404    29  431.939324           R-squared     =  0.0267
-------------+------------------------------           Adj R-squared = -0.0069
       Total |  12869.3548    30  428.978495           Root MSE      =  20.783

------------------------------------------------------------------------------
         DBH |      Coef.   Std. Err.      t    P>|t|     [95% Conf. Interval]
-------------+----------------------------------------------------------------
         CPA |   .0330174   .0370454     0.89   0.380     -.042749    .1087838
       _cons |   35.24616   7.836278     4.50   0.000     19.21917    51.27315
------------------------------------------------------------------------------
```

```
. regress DBH CHM

      Source |       SS       df       MS              Number of obs =      31
-------------+------------------------------           F(  1,    29) =   15.48
       Model |  4478.43357     1  4478.43357           Prob > F      =  0.0005
    Residual |  8390.92127    29  289.342113           R-squared     =  0.3480
-------------+------------------------------           Adj R-squared =  0.3255
       Total |  12869.3548    30  428.978495           Root MSE      =   17.01

------------------------------------------------------------------------------
         DBH |      Coef.   Std. Err.      t    P>|t|     [95% Conf. Interval]
-------------+----------------------------------------------------------------
         CHM |   1.245922   .3166894     3.93   0.000     .5982193    1.893625
       _cons |   3.937859   9.997132     0.39   0.697    -16.50857    24.38429
------------------------------------------------------------------------------
```

```
. regress DBH CrownDiameter

      Source |       SS       df       MS              Number of obs =      31
-------------+------------------------------           F(  1,    29) =    4.11
       Model |  1601.61607     1  1601.61607           Prob > F      =  0.0519
    Residual |  11300.5775    29  389.675085           R-squared     =  0.1241
-------------+------------------------------           Adj R-squared =  0.0939
       Total |  12902.1935    30  430.073118           Root MSE      =   19.74

------------------------------------------------------------------------------
          DBH |      Coef.   Std. Err.      t    P>|t|     [95% Conf. Interval]
--------------+---------------------------------------------------------------
CrownDiameter |   1.589388   .7839747     2.03   0.052    -.0140203    3.192796
        _cons |   29.06208   7.230989     4.02   0.000     14.27305    43.85111
------------------------------------------------------------------------------
```

```
. regress AGB_field DBH

      Source |       SS       df       MS              Number of obs =      31
-------------+------------------------------           F(  1,    29) =  352.28
       Model |   521630376     1   521630376           Prob > F      =  0.0000
    Residual |  42940742.1    29  1480715.25           R-squared     =  0.9239
-------------+------------------------------           Adj R-squared =  0.9213
       Total |   564571118    30  18819037.3           Root MSE      =  1216.8

------------------------------------------------------------------------------
   AGB_field |      Coef.   Std. Err.      t    P>|t|     [95% Conf. Interval]
-------------+----------------------------------------------------------------
         DBH |   201.3275   10.72648    18.77   0.000     179.3894    223.2656
       _cons |  -4789.784   494.8191    -9.68   0.000    -5801.803   -3777.765
------------------------------------------------------------------------------

. regress AGB_field CHM

      Source |       SS       df       MS              Number of obs =      31
-------------+------------------------------           F(  1,    29) =   22.37
       Model |   245825463     1   245825463           Prob > F      =  0.0001
    Residual |   318745656    29  10991229.5           R-squared     =  0.4354
-------------+------------------------------           Adj R-squared =  0.4160
       Total |   564571118    30  18819037.3           Root MSE      =  3315.3

------------------------------------------------------------------------------
   AGB_field |      Coef.   Std. Err.      t    P>|t|     [95% Conf. Interval]
-------------+----------------------------------------------------------------
         CHM |   291.9048   61.72355     4.73   0.000     165.6659    418.1436
       _cons |  -5231.338   1948.466    -2.68   0.012    -9216.397   -1246.278
------------------------------------------------------------------------------

. regress AGB_field CPA

      Source |       SS       df       MS              Number of obs =      31
-------------+------------------------------           F(  1,    29) =    1.34
       Model |  24925485.7     1  24925485.7           Prob > F      =  0.2566
    Residual |   539645633    29  18608470.1           R-squared     =  0.0441
-------------+------------------------------           Adj R-squared =  0.0112
       Total |   564571118    30  18819037.3           Root MSE      =  4313.8

------------------------------------------------------------------------------
   AGB_field |      Coef.   Std. Err.      t    P>|t|     [95% Conf. Interval]
-------------+----------------------------------------------------------------
         CPA |   8.899079   7.689154     1.16   0.257    -6.827007    24.62517
       _cons |   1887.427   1626.499     1.16   0.255    -1439.137    5213.991
------------------------------------------------------------------------------
```

Appendix 6: Sample tally sheet

**Recorder**
**Name** :
**Date** :
**Plot Number** :
**Coordinat** :
**Aspect/ Slope** :
**Crown Cover**

Sapling: 5-9 cm;
H:<2m
Pole: 10-20 cm
Tree: 20 cm up

| No | DBH (cm) | Height (m) | Crown diameter (m) | Species Name | Coordinate | | Remark |
|---|---|---|---|---|---|---|---|
| | | | | | X | Y | |
| 1 | | | | | | | |
| 2 | | | | | | | |
| 3 | | | | | | | |
| 4 | | | | | | | |
| 5 | | | | | | | |
| 6 | | | | | | | |
| 7 | | | | | | | |
| 8 | | | | | | | |
| 9 | | | | | | | |
| 10 | | | | | | | |
| 11 | | | | | | | |
| 12 | | | | | | | |
| 13 | | | | | | | |
| 14 | | | | | | | |
| 15 | | | | | | | |
| 16 | | | | | | | |
| 17 | | | | | | | |
| 18 | | | | | | | |
| 19 | | | | | | | |
| 20 | | | | | | | |
| 21 | | | | | | | |
| 22 | | | | | | | |
| 23 | | | | | | | |
| 24 | | | | | | | |
| 25 | | | | | | | |
| 26 | | | | | | | |
| 27 | | | | | | | |
| 28 | | | | | | | |
| 29 | | | | | | | |
| 30 | | | | | | | |
| 31 | | | | | | | |
| 32 | | | | | | | |
| 33 | | | | | | | |
| 34 | | | | | | | |
| 35 | | | | | | | |
| 36 | | | | | | | |
| 37 | | | | | | | |
| 38 | | | | | | | |
| 39 | | | | | | | |
| 40 | | | | | | | |

Appendix 7: Height, DBH and Biomass from field data

| DBH | Height | Scientific name | Wood Density | Biomass | Carbon Stock |
|---|---|---|---|---|---|
| 20 | 18 | *Schima wallichii* | 1.20 | 439.78 | 206.69 |
| 21 | 30 | *Koompassia malaccensis Maing.* | 1.29 | 868.70 | 408.29 |
| 22 | 15 | *Dryobalanops spp.* | 0.74 | 273.46 | 128.52 |
| 24 | 20 | *Palaquium spp.* | 0.85 | 498.41 | 234.25 |
| 25 | 29 | *Eusideroxylon zwageri T.et B.* | 1.09 | 1005.59 | 472.63 |
| 25 | 16 | *Palaquium spp.* | 0.85 | 432.65 | 203.35 |
| 25 | 15 | *Syzygium spp* | 0.90 | 429.47 | 201.85 |
| 25 | 25 | *Quercus spp.* | 1.10 | 874.84 | 411.18 |
| 26 | 27 | *Quercus spp.* | 1.10 | 1021.93 | 480.31 |
| 27 | 30 | *Quercus spp.* | 1.10 | 1224.50 | 575.52 |
| 27 | 25 | *Palaquium spp.* | 0.85 | 788.50 | 370.60 |
| 27 | 22 | *Artocarpus spp.* | 0.78 | 636.74 | 299.27 |
| 28 | 22 | *Syzygium spp* | 0.90 | 790.13 | 371.36 |
| 29 | 20 | *Quercus spp.* | 1.10 | 941.75 | 442.62 |
| 30 | 35 | *Shorea johorensis Foxw* | 0.86 | 1378.88 | 648.07 |
| 30 | 20 | *Artocarpus spp.* | 0.78 | 714.64 | 335.88 |
| 30 | 37 | *Shorea acuminatissima Sym* | 0.86 | 1457.67 | 685.11 |
| 31 | 23 | *Eusideroxylon zwageri T.et B.* | 1.09 | 1226.30 | 576.36 |
| 32 | 32 | *Shorea acuminatissima Sym* | 0.86 | 1434.39 | 674.16 |
| 33 | 25 | *Quercus spp.* | 1.10 | 1524.33 | 716.43 |
| 33 | 19 | *Shorea johorensis Foxw* | 0.86 | 905.73 | 425.69 |
| 34 | 18 | *Nephelium sp.* | 1.11 | 1175.63 | 552.55 |
| 35 | 43 | *Shorea johorensis Foxw* | 0.86 | 2305.80 | 1083.72 |
| 35 | 30 | *Sindora spp.* | 0.90 | 1683.52 | 791.25 |
| 35 | 45 | *Eusideroxylon zwageri T.et B.* | 1.09 | 3058.39 | 1437.44 |
| 35 | 45 | *Palaquium spp.* | 0.85 | 2384.98 | 1120.94 |
| 38 | 27 | *Quercus spp.* | 1.10 | 2182.94 | 1025.98 |
| 40 | 33 | *Shorea johorensis Foxw* | 0.86 | 2311.27 | 1086.30 |
| 40 | 45 | *Shorea johorensis Foxw* | 0.86 | 3151.73 | 1481.31 |
| 45 | 29 | *Schima wallichii* | 1.20 | 3586.92 | 1685.85 |
| 45 | 29 | *Shorea johorensis Foxw* | 0.86 | 2570.63 | 1208.20 |
| 46 | 27 | *Quercus spp.* | 1.10 | 3198.82 | 1503.45 |
| 50 | 25 | *Shorea johorensis Foxw* | 0.86 | 2735.88 | 1285.86 |
| 52 | 45 | *Shorea johorensis Foxw* | 0.86 | 5326.42 | 2503.42 |
| 55 | 35 | *Shorea assamica Dyer* | 0.95 | 5119.59 | 2406.21 |
| 56 | 25 | *Eusideroxylon zwageri T.et B.* | 1.09 | 4349.71 | 2044.36 |
| 65 | 45 | *Shorea johorensis Foxw* | 0.86 | 8322.53 | 3911.59 |
| 76 | 53 | *Dryobalanops spp.* | 0.74 | 11530.62 | 5419.39 |
| 80 | 54 | *Shorea johorensis Foxw* | 0.86 | 15128.29 | 7110.30 |
| 89 | 33 | *Shorea johorensis Foxw* | 0.86 | 11442.22 | 5377.84 |
| 99 | 38 | *Shorea spp., Hopea spp.* | 0.86 | 16303.10 | 7662.46 |

Appendix 8: Slope correction table

Plot size 500 m²

| Slope% | Radius(m) | Slope% | Radius(m) | Slope% | Radius(m) |
|---|---|---|---|---|---|
| 0 | 12.62 | | | | |
| 1 | 12.62 | 36 | 13.01 | 71 | 13.97 |
| 2 | 12.62 | 37 | 13.03 | 72 | 14.00 |
| 3 | 12.62 | 38 | 13.05 | 73 | 14.04 |
| 4 | 12.62 | 39 | 13.07 | 74 | 14.07 |
| 5 | 12.62 | 40 | 13.09 | 75 | 14.10 |
| 6 | 12.63 | 41 | 13.12 | 76 | 14.14 |
| 7 | 12.63 | 42 | 13.14 | 77 | 14.17 |
| 8 | 12.64 | 43 | 13.16 | 78 | 14.21 |
| 9 | 12.64 | 44 | 13.19 | 79 | 14.24 |
| 10 | 12.65 | 45 | 13.21 | 80 | 14.28 |
| 11 | 12.65 | 46 | 13.24 | 81 | 14.31 |
| 12 | 12.66 | 47 | 13.26 | 82 | 14.35 |
| 13 | 12.67 | 48 | 13.29 | 83 | 14.38 |
| 14 | 12.68 | 49 | 13.31 | 84 | 14.42 |
| 15 | 12.69 | 50 | 13.34 | 85 | 14.45 |
| 16 | 12.70 | 51 | 13.37 | 86 | 14.49 |
| 17 | 12.71 | 52 | 13.39 | 87 | 14.52 |
| 18 | 12.72 | 53 | 13.42 | 88 | 14.56 |
| 19 | 12.73 | 54 | 13.45 | 89 | 14.60 |
| 20 | 12.74 | 55 | 13.48 | 90 | 14.63 |
| 21 | 12.75 | 56 | 13.51 | 91 | 14.67 |
| 22 | 12.77 | 57 | 13.53 | 92 | 14.71 |
| 23 | 12.78 | 58 | 13.56 | 93 | 14.74 |
| 24 | 12.79 | 59 | 13.59 | 94 | 14.78 |
| 25 | 12.81 | 60 | 13.62 | 95 | 14.82 |
| 26 | 12.82 | 61 | 13.65 | 96 | 14.85 |
| 27 | 12.84 | 62 | 13.68 | 97 | 14.89 |
| 28 | 12.86 | 63 | 13.72 | 98 | 14.93 |
| 29 | 12.87 | 64 | 13.75 | 99 | 14.97 |
| 30 | 12.89 | 65 | 13.78 | 100 | 15.00 |
| 31 | 12.91 | 66 | 13.81 | 101 | 15.04 |
| 32 | 12.93 | 67 | 13.84 | 102 | 15.08 |
| 33 | 12.95 | 68 | 13.87 | 103 | 15.12 |
| 34 | 12.97 | 69 | 13.91 | 104 | 15.15 |
| 35 | 12.99 | 70 | 13.94 | 105 | 15.19 |

Source: Y.A. Hussin (2001) from lecture note

Appendix 9: Photos from the field